



Published in final edited form as:

Nature. 2021 March ; 591(7850): 438–444. doi:10.1038/s41586-021-03298-5.

A mechanosensitive peri-arteriolar niche for osteogenesis and lymphopoiesis

Bo Shen¹, Alpaslan Tasdogan¹, Jessalyn M. Ubellacker¹, Jingzhu Zhang¹, Elena D Nosyreva², Liming Du¹, Malea M. Murphy¹, Shuiqing Hu³, Yating Yi⁴, Nergis Kara¹, Xin Liu¹, Shay Guela¹, Yuemeng Jia¹, Vijayashree Ramesh¹, Claire Embree¹, Evann C. Mitchell¹, Yunduo C. Zhao⁵, Lining A. Ju⁵, Zhao Hu⁵, Genevieve M. Crane⁶, Zhiyu Zhao¹, Ruhma Syeda³, Sean J. Morrison^{1,7,*}

¹Children's Research Institute and the Department of Pediatrics, University of Texas Southwestern Medical Center, Dallas, TX 75390, USA.

²Department of Neuroscience, University of Texas Southwestern Medical Center, Dallas, TX 75235, USA.

³Department of Molecular Biology, University of Texas Southwestern Medical Center, Dallas, TX 75390, USA.

⁴Department of Restorative Sciences, School of Dentistry, Texas A&M University, Dallas, TX, 75246, USA

⁵School of Biomedical Engineering, The University of Sydney, Darlington, NSW, 2008, Australia

⁶Robert J. Tomsich Pathology & Laboratory Medicine Institute, Cleveland Clinic, Cleveland, OH, 44106, USA

⁷Howard Hughes Medical Institute, University of Texas Southwestern Medical Center, Dallas, TX 75390, USA

Abstract

Users may view, print, copy, and download text and data-mine the content in such documents, for the purposes of academic research, subject always to the full Conditions of use:http://www.nature.com/authors/editorial_policies/license.html#terms

*Correspondence and requests for materials should be addressed to S.J.M. (Sean.Morrison@UTSouthwestern.edu).

AUTHOR CONTRIBUTIONS

B.S. and S.J.M. conceived the project, designed and interpreted experiments. B.S. performed most of the experiments, with technical assistance and discussions with A.T., J.M.U. and G.M.C. J.Z. and M.M.M. developed immunofluorescence staining protocols. E.D.N. and R.S. performed the electrophysiological recordings measuring Piezo1 channel activity. S.H. assisted in *Listeria* infection experiments. L.D. and N.K. helped to perform flow cytometry. Y.Y. and H.Z. assisted in establishing the hindlimb unloading model and helped with image acquisition. S.G., Y.J. and X.L. assisted B.S. to perform RNA sequencing and analysis. V.R. assisted in ossicle transplantation in NSG mice. E.C.M. and C.E. performed genotyping on mice. L.A.J. and Y.C.Z. provided advice on the mechanical properties of arterioles. Z.Z. performed bioinformatic and statistical analyses. B.S. and S.J.M. wrote the manuscript.

REPORTING SUMMARY

Further information on research design is available in the Nature Research Reporting Summary linked to this paper.

DATA AVAILABILITY

Source data files are provided with this paper. RNA sequencing data have been submitted to the NCBI Sequence Read Archive (SRA), accession number BioProject PRJNA626582.

COMPETING INTERESTS

The authors declare no competing interests.

Leptin Receptor⁺ (LepR⁺) stromal cells in adult bone marrow are a critical source of growth factors, including Stem Cell Factor (SCF), for the maintenance of hematopoietic stem cells (HSCs) and early restricted progenitors¹⁻⁶. LepR⁺ cells are heterogeneous, including skeletal stem cells, osteogenic, and adipogenic progenitors⁷⁻¹², though few markers have been available to distinguish these subsets or to compare their functions. Here we show expression of an osteogenic growth factor, *Ostelectin*^{13,14}, distinguishes peri-arteriolar LepR⁺ cells poised to undergo osteogenesis from peri-sinusoidal LepR⁺ cells poised to undergo adipogenesis (but retaining osteogenic potential). Peri-arteriolar LepR⁺Ostelectin⁺ cells are rapidly dividing, short-lived, osteogenic progenitors that increase in number after fracture and are depleted during aging. Deletion of *Scf* from adult Ostelectin⁺ cells did not affect the maintenance of HSCs or most restricted progenitors but depleted common lymphoid progenitors (CLPs), impairing lymphopoiesis, bacterial clearance, and survival after acute bacterial infection. Peri-arteriolar Ostelectin⁺ cell maintenance required mechanical stimulation. Voluntary running increased, while hindlimb unloading decreased, the frequencies of peri-arteriolar Ostelectin⁺ cells and CLPs. Deletion of the mechanosensitive ion channel, *Piezo1*, from Ostelectin⁺ cells depleted Ostelectin⁺ cells and CLPs. A peri-arteriolar niche for osteogenesis and lymphopoiesis in bone marrow is maintained by mechanical stimulation and depleted during aging.

One Sentence Summary:

A peri-arteriolar niche in the bone marrow for osteogenesis and lymphopoiesis is maintained by mechanical stimulation and is depleted during aging.

HSCs and restricted progenitors are maintained in specialized microenvironments, or niches, in hematopoietic tissues in which stromal cells synthesize the factors they require¹⁵. LepR⁺ cells and endothelial cells are the major sources of factors for HSC maintenance in adult mouse bone marrow, including SCF^{1,3,6}, C-X-C motif chemokine 12 (CXCL12)^{2,16}, and pleiotrophin⁵. LepR⁺ cells are also a critical source of SCF and IL-7 for early restricted progenitors, including CLPs^{4,6}. The bone marrow environment changes with age¹⁷, contributing to the depletion of lymphoid¹⁸ and osteogenic¹⁹ progenitors. However, beyond changes in the abundance of certain kinds of blood vessels^{17,19}, little is known about how the environment changes or what causes the depletion of lymphoid and osteogenic progenitors during aging.

HSCs²⁰⁻²² and erythroid progenitors⁶ localize adjacent to peri-sinusoidal LepR⁺ cells throughout the bone marrow. Single cell RNA sequencing studies showed that peri-sinusoidal LepR⁺ cells appear poised to undergo adipogenic differentiation while peri-arteriolar LepR⁺ cells appear poised to undergo osteogenic differentiation⁹⁻¹². A subset of early lymphoid progenitors resides in an endosteal niche and is maintained by factors from osteoblasts^{2,16,23,24}. Other lymphoid progenitors reside in perivascular niches created partly by LepR⁺ cells^{4,6}, though their precise locations remain uncertain.

***Ostelectin* marks peri-arteriolar LepR⁺ cells**

To test if *Ostelectin* expression resolves functionally distinct subsets of LepR⁺ cells, we generated *Ostelectin-mTomato* (*Oln^{mT}*) knock-in mice (Extended Data Fig. 1a-c). Flow

cytometric analysis of enzymatically dissociated bone marrow cells showed that $0.025 \pm 0.007\%$ of cells were *Oln*-mTomato⁺ (Fig. 1a). *Ostelectin* transcripts were abundant in *Oln*-mTomato⁺ cells but not detected in *Oln*-mTomato⁻ cells (Extended Data Fig. 1d).

Almost all *Oln*-mTomato⁺ cells in the bone marrow were LepR⁺ stromal cells (Fig. 1b), accounting for $16 \pm 1.9\%$ of LepR⁺ cells (Fig. 1c; Extended Data Fig. 1e). Supplementary Table 1 shows the markers used to identify each cell population. *Ostelectin* transcripts were abundant in *Oln*-mTomato⁺LepR⁺ cells but not detected in *Oln*-mTomato⁻LepR⁺ cells (Extended Data Fig. 1f). We did not detect *Oln*-mTomato in bone marrow endothelial cells (Extended Data Fig. 1g).

Deep confocal imaging²¹ of cleared femurs from adult *Oln*^{mT} mice showed that *Oln*-mTomato staining was consistent with anti-Ostelectin antibody staining¹³. In the epiphysis/metaphysis, *Oln*-mTomato was expressed by most hypertrophic chondrocytes and osteoblasts in trabecular bone (Fig. 1d and Extended Data Fig. 1h). In the diaphysis, *Oln*-mTomato was expressed by most osteoblasts and osteocytes in cortical bone (Fig. 1e and Extended Data Fig. 1i) as well as in the periosteum (Extended Data Fig. 1i).

Within the bone marrow, *Oln*-mTomato⁺ cells were exclusively or nearly exclusively peri-arteriolar. Peri-arteriolar LepR⁺ cells were positive for *Oln*-mTomato while peri-sinusoidal LepR⁺ cells were negative for *Oln*-mTomato (Fig. 1f and 1g). Consistent with this, *Oln*-mTomato⁺ cells were associated with Sca-1⁺ arterioles but not Endomucin^{high} sinusoids^{19,25} (Fig. 1h). These *Oln*-mTomato⁺ arterioles were mainly in the diaphysis, in the central marrow and near the endosteum (Extended Data Fig. 2a). In the metaphysis, most arterioles were not surrounded by *Oln*-mTomato⁺ cells (Extended Data Fig. 2b).

We compared the gene expression profiles of CD45⁻Ter119⁻CD31⁻*Scf*-GFP⁺*Oln*-mTomato⁺ peri-arteriolar stromal cells and CD45⁻Ter119⁻CD31⁻*Scf*-GFP⁺*Oln*-mTomato⁻ peri-sinusoidal stromal cells (both cell populations are uniformly LepR⁺). Consistent with single cell RNAseq studies⁹⁻¹², peri-arteriolar *Oln*-mTomato⁺ cells were enriched for the expression of osteogenic genes while peri-sinusoidal *Oln*-mTomato⁻ cells were enriched for adipogenic genes (Extended Data Fig. 2c-d). Both cell populations expressed similar levels of niche (e.g. *Scf* and *Cxcl12*) and mesenchymal genes (e.g. *Lepr* and *Pdgfrb*; Supplementary Table 2).

Ostelectin⁺ cells are short-lived osteogenic progenitors

To investigate the function of Ostelectin⁺ cells, we inserted *iCreER* into the *Ostelectin* locus to generate *Ostelectin*^{*iCreER*} (*Oln*^{*iCreER*}) mice (Extended Data Fig. 2e-g). Consistent with the *Oln*-Tomato expression pattern, the *Oln*^{*iCreER*} allele recombined in peri-arteriolar, but not peri-sinusoidal, stromal cells (Extended Data Fig. 2h) as well as in hypertrophic chondrocytes (Extended Data Fig. 2i), osteoblasts (Extended Data Fig. 2i), and osteocytes (Extended Data Fig. 2j). We found that $91 \pm 3.0\%$ and $12 \pm 3.3\%$ of colony-forming units-fibroblast (CFU-F) formed by *Lepr*^{cre/+}; *Rosa26*^{loxP-tdTomato/+} cells and *Oln*^{*iCreER*};⁺; *Rosa26*^{loxP-tdTomato/+} cells, respectively, were Tomato⁺ (Fig. 2a). Furthermore, $11 \pm 2.4\%$ of *Oln*-Tomato⁻LepR⁺ stromal cells but only $5.2 \pm 1.3\%$ of *Oln*-mTomato⁺LepR⁺ cells formed

CFU-F (Fig. 2b). These data suggest skeletal stem cells were enriched among Ostelectin negative LepR⁺ cells.

When stimulated to differentiate, CFU-F formed by *Oln*-Tomato⁺LepR⁺ stromal cells gave rise to significantly more osteoblasts and significantly fewer adipocytes than CFU-F formed by *Oln*-Tomato⁻LepR⁺ cells (Fig. 2c and 2d). When we assessed spontaneous differentiation, the colonies formed by *Oln*-Tomato⁺LepR⁺ cells contained only osteoblasts while colonies formed by *Oln*-Tomato⁻LepR⁺ cells contained osteoblasts and adipocytes (Fig. 2e). *Oln*-Tomato⁺LepR⁺ peri-arteriolar cells were thus enriched for osteogenic progenitors while *Oln*-Tomato⁻LepR⁺ peri-sinusoidal cells were enriched for multipotent cells. *Oln*-mTomato⁺LepR⁺ cells were also more mitotically active (Fig. 2f).

In two month-old *Oln^{mT/iCreER}; Rosa26^{loxP-EGFP}* mice, 96±1.8% of *Oln*-mTomato⁺ cells were EGFP⁺ 3 days after tamoxifen treatment, indicating high recombination efficiency in peri-arteriolar stromal cells (Fig. 2g). We did not detect EGFP in *Oln*-mTomato⁻ cells. Two months later, only 1.9±2.2% of *Oln*-mTomato⁺ cells were EGFP⁺ (Fig. 2g). Three days after tamoxifen treatment of *Oln^{iCreER}; Rosa26^{loxP-tdTomato}* mice, 35±5.4% of LepR⁺ cells were Tomato⁺ (Fig. 2h). These cells were present around arterioles throughout the diaphysis (Extended Data Fig. 2h). However, two months later, only 2.2±3.5% of LepR⁺ cells were Tomato⁺ (Fig. 2h). Peri-arteriolar *Ostelectin*⁺ cells are, thus, rapidly dividing and short-lived progenitors.

Ostelectin⁺ cells are fated to form bone, not fat

We performed lineage tracing in two month-old *Oln^{iCreER}; Rosa26^{loxPtd-Tomato}*; *Colla1*2.3-EGFP* mice²⁶. Although Ostelectin is expressed by osteoblasts (Fig. 1d and 1e; Extended Data Fig. 2i), only around 20% of *Colla1*2.3-EGFP*⁺ bone-lining cells were Tomato⁺ in these mice 3 days after tamoxifen treatment, indicating low recombination efficiency in osteoblasts (Fig. 2i). One month after tamoxifen treatment almost all *Colla1*2.3-EGFP*⁺ bone-lining cells were Tomato⁺, then the percentage continuously declined (Fig. 2i). Given that endosteal osteoblasts have little proliferative potential²⁷ and are constantly regenerated from progenitors in the bone marrow²⁸, this suggests that many new osteoblasts arise from peri-arteriolar *Ostelectin*⁺ cells, particularly in the diaphysis.

We fate-mapped differentiated osteoblasts by treating 2-month-old *Colla1-creER*; *Rosa26^{loxP-tdTomato}*; *Colla1*2.3-EGFP*⁺ mice with tamoxifen. *Colla1-creER* does not recombine in LepR⁺ stromal cells¹. Tomato was expressed by 92±3.2% of *Colla1*2.3-EGFP*⁺ osteoblasts 3 days after tamoxifen treatment but by only 24±7.4% of *Colla1*2.3-EGFP*⁺ osteoblasts 1 month later (Extended Data Fig. 2k). Endosteal osteoblasts are, therefore, short-lived and constantly regenerated from undifferentiated progenitors.

We sublethally irradiated *Oln^{iCreER}; Rosa26^{loxP-tdTomato}* mice 3 days after tamoxifen treatment and examined the bone marrow 14 days later. We observed large numbers of adipocytes but none were Tomato⁺ (Extended Data Fig. 3a).

We also compared the ability of LepR⁺*Ostelectin*⁺ and LepR⁺*Ostelectin*⁻ cells to form bony ossicles in vivo²⁹. Thirty three of 80 denatured collagen sponges seeded with the

progeny of cultured LepR⁺Osteolectin⁻ cells formed ossicles after transplantation into NSG mice, 21 containing hematopoietic marrow and adipocytes (Fig. 2j; Extended Data Fig. 3b). In contrast, 36 out of 80 sponges seeded with the progeny of cultured LepR⁺Osteolectin⁺ cells formed ossicles but none contained hematopoietic marrow or adipocytes (Fig. 2j; Extended Data Fig. 3b). LepR⁺Osteolectin⁺ cells are osteogenic progenitors with little skeletal stem cell or adipogenic activity.

We performed femur fractures 3 days after tamoxifen in 2-month-old *OlnⁱCreER/+*; *Rosa26^{loxP-tdTomato/+}*; *Col1a1*2.3-EGFP⁺* mice. Two weeks later, we observed a substantial increase in the number of LepR⁺ cells and the percentage of LepR⁺ cells that were *Oln-Tomato⁺* in the bone marrow (Fig. 2k and 2l). Within the callus at the fracture site, *Oln-Tomato⁺* cells accounted for 82±10% of *Col1a1*2.3-EGFP⁺* osteoblasts. *Osteolectin⁺* cells, thus, expand in number after fracture and form most of the osteoblasts that contribute to bone regeneration.

A peri-arteriolar niche for lymphoid progenitors

LepR⁺Osteolectin⁺ peri-arteriolar stromal cells and LepR⁺Osteolectin⁻ peri-sinusoidal stromal cells were uniformly positive for *Scf*-GFP, with similar levels of expression (Fig. 3a–b). *Scf* deletion from Osteolectin⁺ cells in adult *OlnⁱCreER/+*; *Scf^{fl/fl}* mice did not significantly affect bone marrow or spleen cellularity (Fig. 3c), blood cell counts (Extended Data Fig. 3c–e), or the frequencies of differentiated B, T, myeloid, megakaryocyte, or erythroid lineage cells in the bone marrow or spleen (Extended Data Fig. 3f–j). Consistent with the localization of HSCs to sinusoidal blood vessels^{20–22}, *Scf* deletion in peri-arteriolar *Osteolectin⁺* cells did not significantly affect HSC or MPP frequency in the bone marrow (Fig. 3d) or spleen (Extended Data Fig. 3k) or the reconstituting capacity of bone marrow cells in irradiated mice (Extended Data Fig. 3l). *Scf* deletion from *Osteolectin⁺* cells also did not significantly affect the frequencies of granulocyte-macrophage progenitors (GMPs), megakaryocyte-erythroid progenitors (MEPs), or common myeloid progenitors (CMPs) but did significantly reduce the frequency of CLPs in the bone marrow (Fig. 3d). The flow cytometry gates used to sort each stem/progenitor cell population are shown in Extended Data Fig. 4.

This suggested *Osteolectin⁺* cells might create a peri-arteriolar niche for CLPs. Although *OlnⁱCreER* also recombined in a minority of osteoblasts (Fig. 2i), osteoblasts do not express *Scf*^{1,9–12} and deletion of *Scf* from osteoblasts does not affect CLP frequency¹. Consistent with these studies, we did not detect *Scf*-GFP expression by Osteolectin⁺ osteoblasts, osteocytes, or hypertrophic chondrocytes (Extended Data Fig. 3m–n and Extended Data Fig. 5a–d). We were unable to find non-peri-arteriolar Osteolectin⁺ cells in the bone marrow that express *Scf*.

Consistent with a peri-arteriolar niche for lymphoid progenitors, 35% of IL7Rα⁺Lineage⁻ cells (which are mainly CLPs², Extended Data Fig. 4e) were within 5 μm of peri-arteriolar Osteolectin⁺ cells (Fig. 3e and 3f; 18-fold more likely than other hematopoietic cells). Consistent with the existence of an endosteal niche for CLPs^{2,16,23,24}, another 28% of IL7Rα⁺Lineage⁻ cells were within 5 μm of the endosteal surface (Fig. 3f; 7-fold more likely

than other hematopoietic cells). Deletion of *Scf* from Ostelectin⁺ cells significantly reduced the frequency of peri-arteriolar, but not endosteal, IL7Rα⁺Lineage⁻ cells (Fig. 3g). A subset of early lymphoid progenitors thus resides adjacent to arterioles and depends upon SCF from Ostelectin⁺ cells.

To more fully assess the role of this niche in lymphopoiesis, we treated *Oln^{iCreER/+}; Scf^{fl/fl}* mice and littermate controls with tamoxifen for 2 months, beginning at 2 months of age. We did not observe any effect on the frequencies of HSCs, MPPs, GMPs, MEPs, or CMPs in the bone marrow (Extended Data Figure 5e); however, *Oln^{iCreER/+}; Scf^{fl/fl}* mice did exhibit a broad depletion of lymphoid progenitors including CLPs, Pre-proB cells, and PreB cells in the bone marrow (Fig. 3h) as well as early thymic progenitors (ETPs) and double negative (DN1 and DN2) thymocytes (Fig. 3i and 3j). Nonetheless, the numbers of differentiated B and T cells were normal in *Oln^{iCreER/+}; Scf^{fl/fl}* mice under steady-state conditions (Extended Data Fig. 5f and 5g).

Fracture did not significantly affect the frequencies of HSCs and MPPs but did increase the frequencies of *Oln*-mTomato⁺ cells and CLPs in the bone marrow (Extended Data Fig. 5h and 5i). Moreover, IL7Rα⁺Lineage⁻ cells were significantly more likely to be associated with Ostelectin⁺ arterioles in fractured as compared to control bones (Extended Data Fig. 5j). Conditional deletion of *Scf* from Ostelectin⁺ cells blocked the increase in CLPs after fracture without affecting the frequency of *Oln*-mTomato⁺ cells (Extended Data Fig. 5h and 5i).

To test if increasing bone mass is sufficient to promote the expansion of Ostelectin⁺ cells or CLPs in the bone marrow we administered Parathyroid Hormone (PTH) to mice daily for a month. PTH treatment significantly increased bone volume (Extended Data Fig. 6a and 6b) but decreased the frequencies of Ostelectin⁺ stromal cells and CLPs in the bone marrow (Extended Data Fig. 6c and 6d). Increased bone volume was, therefore, not sufficient to increase Ostelectin⁺ cells and CLPs.

Aging depletes peri-arteriolar Ostelectin⁺ cells

The frequency of *Oln*-mTomato⁺ cells in the bone marrow diaphysis declined significantly during aging (Extended Data Fig. 6e) even though the overall frequency of LepR⁺ cells did not change (Extended Data Fig. 6f). In 2-month-old mice, nearly all arterioles in the diaphysis were surrounded by Ostelectin⁺ cells (Fig. 1h and 3a). In 18-month-old mice, about half of peri-arteriolar regions in the diaphysis lacked Ostelectin⁺ cells, in the central marrow and near the endosteum (Extended Data Fig. 6g). CLPs were also depleted during aging (Extended Data Fig. 6h). In contrast, HSC and MPP frequency increased during aging^{18,30} and GMPs, CMPs, and MEPs did not significantly change (Extended Data Fig. 6i–m). The percentage of IL7Rα⁺Lineage⁻ cells associated with arterioles declined during aging (Extended Data Fig. 6n), particularly around arterioles that lacked Ostelectin⁺ cells (Extended Data Fig. 6o and 6p). This suggests that the age-related decline in lymphoid progenitors may be caused partly by the loss of Ostelectin⁺ cells.

Peri-arteriolar niches promote the response to infection

We tested if the peri-arteriolar niche was necessary for lymphopoiesis after acute infection with a bacterium whose clearance depends upon T and B cells^{31,32}. Three days after tamoxifen treatment, *Oln^{iCreER/+}; Scf^{fl/fl}* mice and littermate controls were administered *Listeria monocytogenes* by oral gavage. In the absence of *Listeria*, B and T cell counts were similar in *Oln^{iCreER/+}; Scf^{fl/fl}* mice and littermate controls (Extended Data Fig. 7a and 7b). After *Listeria* infection, B and T cell counts significantly increased in the spleens of control, but not *Oln^{iCreER/+}; Scf^{fl/fl}* mice and bacterial CFUs were significantly increased in the spleens of *Oln^{iCreER/+}; Scf^{fl/fl}* mice as compared to controls (Extended Data Fig. 7a–c). Ostelectin⁺ peri-arteriolar niches thus appeared to be required to augment lymphopoiesis and to clear bacteria after acute infection.

We also administered *Listeria* intraperitoneally. Relative to controls, *Oln^{iCreER/+}; Scf^{fl/fl}* mice had fewer CLPs (Fig. 3k) and Pre-proB cells in the bone marrow (Extended Data Fig. 7d), as well as ETPs and DN1 cells in the thymus (Extended Data Fig. 7e) at 5 and 10 days after infection. We also observed reduced numbers of B, T, and NK1.1⁺CD3⁻ natural killer (NK) cells (Extended Data Fig. 7f–i and 7l–m), impaired *Listeria* clearance (Extended Data Fig. 7j and 7n), and reduced survival (Fig. 3l). We observed no change in IFN- γ levels in T cells from *Oln^{iCreER/+}; Scf^{fl/fl}* as compared to control mice (Extended Data Fig. 7k) suggesting normal T cell activation. The peri-arteriolar niche is thus required for the maintenance of normal numbers of lymphoid progenitors and lymphocytes during the response to acute bacterial infection.

Mechanical stimulation maintains peri-arteriolar niches

To test if exercise could restore peri-arteriolar niches in aging bone marrow, running wheels were placed in the cages of 18-month-old *Oln^{mT/+}* mice for 4 weeks. Voluntary running increased bone mineral density (Extended Data Fig. 8a) and cortical bone thickness (Fig. 4a), as well as the frequencies of *Oln*-mTomato⁺ cells (Fig. 4b) and CLPs (Fig. 4c) relative to non-running control mice. Voluntary running did not significantly affect the frequencies of HSCs, MPPs, GMPs, MEPs, or CMPs (Fig. 4c). Voluntary running increased CLP frequency in load-bearing long bones (Fig. 4c) but not in the calvarium of the same mice (Extended Data Fig. 8b). Voluntary running thus appeared to promote the expansion of peri-arteriolar niches in load-bearing bones.

To test if mechanical loading is required for Ostelectin⁺ cell maintenance, we suspended the hindlimbs of 2-month-old *Oln^{mT/+}* mice for two weeks to reduce mechanical loading on the hindlimbs while they walked on their forelimbs³³ (Extended Data Fig. 8c). In the forelimbs, we observed no significant effects on bone mineral density, cortical bone thickness, or the frequencies of *Oln*-mTomato⁺ cells, CLPs, HSCs, MPPs, GMPs, MEPs, or CMPs in the bone marrow (Extended Data Fig. 8d–g). In contrast, the femurs of suspended mice exhibited significantly reduced bone mineral density (Extended Data Fig. 8h), cortical bone thickness, *Oln*-mTomato⁺ cell frequency, and CLP frequency relative to control mice (Fig. 4d–f). The depletion of Ostelectin⁺ cells after unloading may have been caused by reduced proliferation as we observed reduced BrdU incorporation (Fig. 4g). We did not

detect any effect of hindlimb suspension on the frequencies of HSCs, MPPs, GMPs, MEPs, or CMPs (Fig. 4f). Hindlimb unloading thus reduced the frequencies of *Oln*-mTomato⁺ cells and CLPs, suggesting that mechanical loading is required for the maintenance of peri-arteriolar niches.

Ostelectin⁺ cells expressed the stretch-induced ion channel Piezo1^{34,35} by gene expression profiling and western blot (Fig. 4k). Mechanical loading promotes bone formation and increases skeletal bone mass³⁶, partly by promoting Piezo1 signaling in mesenchymal progenitors during development³⁷ and in osteoblasts during adulthood^{34,35,38}. To test if mechanical stimulation elicits Piezo-like channel activity in Ostelectin⁺ cells, we sorted LepR⁺Ostelectin⁺ cells into culture and performed patch clamp recordings with negative applied pressures^{37,39} (Fig. 4h and Extended Data Fig. 8i). We observed Piezo-like channel properties in Ostelectin⁺ cells that recapitulated previously reported Piezo1 single channel conductance and pressure-dependent activity³⁷. The channels were sensitized by Yoda1, a pharmacological agonist of Piezo1⁴⁰. The calculated P_{1/2} (pressure at which half of the channels are open) was -35 mm Hg with Yoda1 and -45 mmHg without Yoda1 (Fig. 4i). Pressure-dependent and Yoda1-dependent channel activity were not observed in Ostelectin⁺ cells from *Oln^{mTl}iCreER*; *Piezo1^{fl/fl}* mice (Extended Data Fig. 8j and 8k). A Yoda1-induced calcium influx was observed in Ostelectin⁺ cells from control, but not *Oln^{mTl}iCreER*; *Piezo1^{fl/fl}* mice (Fig. 4j).

Piezo1 deletion from *Ostelectin⁺* cells at 2 months of age significantly reduced *Piezo1* transcript and protein levels in Ostelectin⁺ cells (Extended Data Fig. 8l; Fig. 4k) as well as bone mineral density (Extended Data Fig. 8m), cortical bone thickness (Fig. 4l), *Oln*-mTomato⁺ cell frequency (Fig. 4m), and CLP frequency (Fig. 4n). The depletion of Ostelectin⁺ cells after *Piezo1* deletion may have been caused by reduced proliferation as we observed reduced BrdU incorporation (Extended Data Fig. 8n). The percentage of CLPs associated with arterioles also significantly declined after *Piezo1* deletion (Extended Data Fig. 8o). We did not detect any effect of *Piezo1* deletion on the frequencies of HSCs, MPPs, GMPs, MEPs, or CMPs (Fig. 4n). The phosphorylation of calcium/calmodulin-dependent protein kinase II (CaMKII), a downstream mediator of Piezo signaling, was reduced in *Piezo1* deficient as compared to control Ostelectin⁺ cells (Fig. 4k). Piezo1 thus acts within Ostelectin⁺ cells to maintain a peri-arteriolar niche for osteogenic and lymphoid progenitors.

We conditionally deleted *Piezo1* in osteoblasts using *Coll1a1*-creER and in all LepR⁺ cells using *Lepr^{cre}*. *Coll1a1*-creER; *Piezo1^{fl/fl}*; *Oln^{mTl}*⁺ mice had reduced bone mass as compared to sex-matched littermate controls (Extended Data Fig. 8p and 8q), consistent with Piezo1 function in osteoblasts^{34,35,38}. However, there were no differences between *Coll1a1*-creER; *Piezo1^{fl/fl}*; *Oln^{mTl}*⁺ and control mice in the frequencies of Ostelectin⁺LepR⁺ bone marrow cells (Extended Data Fig. 8r) or hematopoietic stem/progenitor cells (Extended Data Fig. 8s). Therefore, the maintenance of peri-arteriolar Ostelectin⁺ cells and CLPs does not require mechanical stimulation of osteoblasts.

We also examined *Lepr^{cre/+}*; *Piezo1^{fl/fl}*; *Oln^{mTl}*⁺ mice, in which *Piezo1* was deleted from both peri-arteriolar LepR⁺Ostelectin⁺ cells and peri-sinusoidal LepR⁺Ostelectin⁻ cells.

The bone mass and CLP depletion phenotypes were not more severe in *Lepr^{cre/+}; Piezo1^{fl/fl}; Oln^{mT/+}* mice (Extended Data Fig. 8t–w) as compared to *Oln^{mT/iCreER}; Piezo1^{fl/fl}* mice (Fig. 4l–n). Moreover, *Piezo1* deletion from all LepR⁺ cells had no effect on the frequencies of HSCs, MPPs, GMPs, MEPs, or CMPs (Extended Data Fig. 8w). This suggests that mechanical stimulation is not required for the maintenance of peri-sinusoidal niches. Mechanical forces may selectively regulate the maintenance of peri-arteriolar niches.

Finally, we tested if mechanosensation in Ostelectin⁺ cells promoted the response to acute infection. Three days after tamoxifen treatment, *Oln^{mT/iCreER}; Piezo1^{fl/fl}* mice and littermate controls were administered oral *Listeria*. Absent *Listeria*, B and T cell counts were similar in the spleens of *Oln^{mT/iCreER}; Piezo1^{fl/fl}* mice and controls (Extended Data Fig. 8x and 8y). After *Listeria* infection, B and T cells were significantly reduced and bacterial CFUs were significantly increased in the spleens of *Oln^{mT/iCreER}; Piezo1^{fl/fl}* as compared to control mice (Extended Data Fig. 8x–z). Loss of Piezo1 from Ostelectin⁺ cells, thus, impaired lymphopoiesis and bacterial clearance after acute infection.

Arteriolar endothelial cells may also regulate the maintenance of lymphoid progenitors in peri-arteriolar niches as deletion of Notch ligand from arteriolar endothelial cells impairs lymphopoiesis⁹. Arterioles may be particularly effective at transmitting movement-induced mechanical stimuli from the bone into the marrow because they are thicker and stiffer walled than sinusoids⁴¹ and often enter the bone marrow by passing through cortical bone^{42,43}.

METHODS

Mice

All mouse experiments complied with all relevant ethical regulations and were performed according to protocols approved by the Institutional Animal Care and Use Committees at UT Southwestern Medical Center (protocol 2017–101896) and Texas A&M Health Science Center (2018–0217-CD). All mice were maintained on a C57BL/Ka background, including *Lepr^{cre}* (ref⁴⁴), *Rosa26-CAG-loxp-stop-loxp-tdTomato* (Ai14)⁴⁵, *Rosa26-CAG-loxp-stop-loxp-EGFP* (Ai47)⁴⁶, *Coll1a1*2.3-EGFP*²⁶, *Piezo1^{fllox}* (ref⁴⁷), *Scf^{fllox}* and *Scf^{GFP}* (ref¹) mice. To generate *Oln^{mT}* and *Oln^{iCreER}* mice, CleanCap Cas9 mRNA (TriLink) and sgRNAs (transcribed using MEGAshortscript Kit (Ambion) and purified using the MEGAclean Kit (Ambion)), and recombineering plasmids were microinjected into C57BL/Ka zygotes. Chimeric mice were genotyped by restriction fragment length polymorphism analysis and insertion of the *mTomato* sequence⁴⁸ into the correct locus was confirmed by Southern blotting and sequencing of the targeted allele. Founders were mated with C57BL/Ka mice to obtain germline transmission then backcrossed with wild-type C57BL/Ka mice for at least three generations before analysis. To induce Cre recombinase activity, unless otherwise indicated, *Oln^{iCreER/+}* mice received a daily intraperitoneal injection of 1mg of tamoxifen dissolved in corn oil for 5 days. All mice were housed in specific pathogen-free animal care facilities under a 12h:12h light/dark cycle with a temperature of 65–75°F and humidity of 40–60%.

Genotyping Primers

Primers for genotyping *Oln^{mT}* mice were 5'-TCT GGG AGA CCA CAG AGA CTC AAGG, 5'-AAA GAC AGA AGG CAC AAC TAG AGGC, 5'-CAA TTC CGT GGT GTT GTC GGG GAA ATC ATC, and 5'-CAC TGT GAA AAG ACA GAA GGC ACA ACT AGAG. Primers for genotyping *Oln^{iCreER}* mice were 5'-TCA AGA GTT TAA CCC ACT GAA CTT CAT AGA, 5'-CTC GTT AGA GCA GTA GTG TGT TAG TGAA, 5'-TGG GTA GAC CCA AGG CGG GA, and 5'-GGA GGG CAG GCA GGT TTT GGT.

Flow cytometry

Bone marrow hematopoietic cells were isolated by flushing the long bones with Ca²⁺- and Mg²⁺-free HBSS (HBSS-free) with 2% heat-inactivated bovine serum. Spleen cells were obtained by crushing the spleen between two glass slides. The cells were dissociated into a single cell suspension by gently passing them through a 25-gauge needle and then filtering through 70- μ m nylon mesh. HSCs were isolated using anti-CD150 (TC15-12F12.2), anti-CD48 (HM48-1), anti-Sca1 (E13-161.7), and anti-c-kit (2B8) along with the following antibodies against lineage markers: anti-Ter119, anti-B220 (6B2), anti-Gr1 (8C5), anti-CD2 (RM2-5), anti-CD3 (17A2), anti-CD5 (53-7.3) and anti-CD8 (53-6.7). Hematopoietic progenitors were isolated with the lineage markers anti-Ter119, anti-B220, anti-Gr1, anti-CD2, anti-CD3, anti-CD5, and anti-CD8 as well as additional antibodies against CD34 (RAM34), CD135 (FLT3) (A2F10), CD16/32 (Fc γ R) (clone 93), CD127 (IL7Ra) (A7R34), CD43 (1B11), CD24 (M1/69), IgM (II/41), CD44 (IM7), and CD25 (PC61.5). DAPI was used to exclude dead cells. The markers used to identify each cell population in this study are summarized in Supplementary Table 1. All antibodies were used at 1:200 dilution unless otherwise specified.

For flow cytometric analysis of stromal cells, bone marrow was flushed using HBSS-free with 2% bovine serum. Then whole bone marrow was digested with type I collagenase (3 mg/ml), dispase (4 mg/ml) and DNase I (1 U/ml) at 37°C for 30 min as described previously¹⁴. Samples were then stained with antibodies and analyzed by flow cytometry. Goat-anti-LepR-biotin (AF497), anti-CD45 (30F-11), anti-CD31 (clone 390) and anti-TER119 antibodies were used to isolate LepR⁺ cells. For analysis of bone marrow endothelial cells, mice were intravenously injected with 10 μ g per mouse of eFluor660-conjugated anti-VE-cadherin antibody (BV13, eBiosciences). Ten minutes later, the long bones were removed and bone marrow was flushed, digested and stained as above. Samples were analyzed using FACS Aria or FACSCanto II flow cytometers and FACSDiva 8.0 (BD) or FlowJo v10.6.1 (Tree Star) software.

Immunostaining of bone sections

Freshly dissected mouse femurs were fixed in 4% paraformaldehyde overnight. Bones were decalcified in phosphate-buffered saline (PBS) with 10% EDTA and 30% sucrose for 5 days. Bones were sectioned in 12 μ m slices using the CryoJane tape-transfer system (Leica). Sections were blocked in PBS with 5% normal donkey serum (Jackson Immuno) for 1 hour and then stained overnight with chicken-anti-GFP (Aves), rabbit-anti-tomato (Takara), and goat-anti-LepR-biotin (R&D Systems). Donkey anti-chicken Alexa Fluor 488 (Jackson Immuno), donkey anti-goat Alexa Fluor 488 (Jackson Immuno), donkey anti-goat Alexa

Fluor 555 (Invitrogen) and donkey anti-rabbit Alexa Fluor 647 (Jackson Immuno) were used as secondary antibodies. Slides were mounted with Prolong Gold anti-fade medium (Invitrogen). To identify CLPs, mice were intravenously injected with 2 μ g Alexa Fluor 647 anti-IL7R α (A7R34, Biolegend). After 5 minutes, the mice were killed and long bones were dissected, fixed, sectioned and stained with antibodies against Lineage markers (anti-CD2, CD3, CD5, CD8, TER119, GR1 and B220). Images were acquired with a Zeiss LSM780 or a Leica SP8 confocal microscope. Confocal images were processed and analyzed using Zeiss Zen-2 or Leica LAS X.

Deep imaging of half bones

Femurs were longitudinally cut in half, then stained, and deep imaged as described previously²¹. The staining solution contained 10% DMSO, 0.5% IgePal630 (Sigma), and 5% donkey serum (Jackson Immuno) in PBS. Half bones were stained for 3 days at room temperature with primary antibodies. Then specimens were washed 3 times in PBS at room temperature for one day and put into staining solution containing secondary antibodies for 3 days followed by a one-day wash. Antibodies used for whole mount staining included chicken anti-GFP (Aves Labs, 1:200), anti-tdTomato (Takara, 1:200), Alexa Fluor 647-AffiniPure F(ab')₂ Fragment Donkey Anti-Chicken IgY (1:250), Alexa Fluor 488-AffiniPure F(ab')₂ Fragment Donkey Anti-Rabbit IgG (1:250), Alexa Fluor 488-AffiniPure F(ab')₂ Fragment Donkey Anti-Rabbit IgG (all from Jackson ImmunoResearch, 1:250), and 555-conjugated donkey anti-goat antibody (Invitrogen, 1:250). Images were acquired using a Leica SP8 confocal microscope. Images were rendered in 3D and analyzed using Bitplane Imaris v7.7.1.

CFU-F and *in vitro* differentiation assay

Freshly dissociated bone marrow cells were plated at clonal density in 6-well plates pre-coated with 100 ng/ml of fibronectin (Sigma) overnight. The cells were cultured in DMEM-low glucose (Gibco) plus 20% fetal bovine serum (Sigma), 10mM ROCK inhibitor Y-27632 (Selleck), and 1% penicillin/streptomycin (Invitrogen) at 37°C in gas-tight chambers (Billups-Rothenberg) flushed with 1% O₂ and 6% CO₂ (balance Nitrogen) to maintain physiological oxygen levels that promoted survival and proliferation⁴⁹. To count CFU-F colonies, the cultures were stained with 0.1% Toluidine blue in 4% formalin eight days after plating. Osteogenic, adipogenic, and chondrogenic differentiation were assessed using StemPro Differentiation kits (Gibco).

Quantitative reverse transcription PCR

For quantitative reverse transcription PCR (qPCR), cells were flow cytometrically sorted from enzymatically dissociated bone marrow into Trizol (Invitrogen). RNA was extracted and reverse transcribed into cDNA using SuperScript III (Invitrogen) and random primers. qPCR was performed using a Roche LightCycler 480. The primers used for qPCR analysis included mouse *Ostelectin*: 5'-AGG TCC TGG GAG GGA GTG-3' and 5'-GGG CCT CCT GGA GAT TCT T-3'; *Actb*: 5'-GCT CTT TTC CAG CCT TCC TT-3' and 5'-CTT CTG CAT CCT GTC AGC AA-3'.

Long-term competitive reconstitution assays

Recipient mice were irradiated using an XRAD 320 X-ray irradiator (Precision X-Ray Inc.) with two doses of 540 rad at least 4 hours apart. C57BL/Ka (CD45.1/CD45.2 heterozygous) mice were used as recipients. 500,000 unfractionated bone marrow cells from donor (CD45.2) and competitor (CD45.1) mice were mixed and injected intravenously through the retro-orbital venous sinus. Recipient mice were bled from 4 to 16 weeks after transplantation to examine the levels of donor-derived myeloid, B, and T cells in their blood. Red blood cells were then lysed with ammonium chloride potassium buffer before antibody staining. The antibodies used to analyze donor chimerism in the blood were anti-CD45.1 (A20), anti-CD45.2 (104), anti-Gr1 (8C5), anti-Mac1 (M1/70), anti-B220 (6B2) and anti-CD3 (KT31.1).

Bone fracture and ossicle formation

As described¹³, a stainless steel wire was inserted into the intramedullary canal of the femur through the knee after anesthesia, and the femur was fractured mid-diaphysis by 3-point bending. Buprenorphine was injected every 12 hours up to 72 hours after the surgery. Mice were analyzed 2 weeks after the surgery, using the contralateral femur as an internal control.

As described previously^{13,29}, 2×10^6 cultured mouse primary CFU-F cells were seeded into collagen sponges (Gelfoam), incubated at 37°C for 90 min, and then transplanted subcutaneously into NOD-SCID IL2R $\gamma^{-/-}$ (NSG) mice. The ossicles formed by these cells were analyzed eight weeks after transplantation by cryosectioning, Hematoxylin and Eosin staining.

MicroCT analysis

Femurs from sex-matched littermates were fixed in 4% PFA overnight at 4°C, then the bones were washed four times with 70% ethanol and stored in 70% ethanol until scanned using a Scanco Medical μ CT 35. Femurs were scanned at an isotropic voxel size of 3.5 μ m, with peak tube voltage of 55 kV and current of 0.145 mA (μ CT 35; Scanco). A three-dimensional Gaussian filter ($s = 0.8$) with a limited, finite filter support of one was used to suppress noise. A threshold of 263–1000 was used to segment mineralized bone from air and soft tissues. Cortical bone parameters were measured by analyzing 100 slices in mid-diaphysis femurs.

RNA-seq analysis

Cells were sorted into RLT buffer (Qiagen RNAeasy Plus Micro kit) and RNA was purified according to the manufacturer's instructions. RNA quality was validated using a Pico Bioanalyzer. Libraries were generated using SMARTer Stranded Total RNA-Seq kit – Pico Input Mammalian (Clontech). Library fragment size was measured using D1000 Screen Tape (Agilent) and RNA was quantified using the Qubit RNA assay kit (Life Technologies). Libraries were sequenced using an Illumina NextSeq 500. The quality of RNA-seq raw reads was checked using FastQC 0.11.5. Raw reads were trimmed using Cutadapt 2.3 and mapped to the Ensembl GRCm38 mouse genome using TopHat 2.1.1 with Bowtie2 2.2.3. Mapped reads were quality-filtered using SAMtools 1.9.0 and quantified using HTSeq 0.9.1. Differential expression was assessed using DESeq2 1.24.0 with R 3.6.1. Gene set

enrichment analysis of the filtered, DESeq2-normalized counts was performed using GSEA 4.0.3 with the osteogenesis gene list PAMM-026Z and the adipogenesis gene list PAMM-049Z from Qiagen's RT² Profiler PCR Array.

Voluntary running and hindlimb unloading

Mice were individually housed in standard polycarbonate mouse cages (Fisher Scientific) containing a 4.75" diameter stainless steel running wheel for 4 weeks. To mechanically unload mouse hindlimbs, 8-week-old mice were outfitted with tail harnesses and suspended from an overhead pulley system in customized cages, as described previously³³ (see schematic in Extended Data Fig. 8c). The mice ambulated within the cage using their forelimbs, which remained in contact with the cage floor, but their hindlimbs were suspended in the air and consequently could not generate ground reaction forces. Control mice were housed individually with tail harnesses attached to the overhead pulley system as well, but with both forelimbs and hindlimbs in contact with the cage floor. Food and water were provided on the cage floor. Mice were suspended continuously for 2 weeks, then analyzed.

Listeria infection

Listeria monocytogenes strain 10403S was freshly inoculated onto a brain-heart infusion (BHI) agar plate. A single colony was chosen and expanded in BHI broth at 37°C with shaking at 200 rpm. For infection, bacteria were sub-cultured and grown to log phase (OD₆₀₀ = 0.6–1) on the day of infection, washed, and resuspended in PBS. Mice were administered 2×10⁹ CFU of *Listeria* by oral gavage, or 2×10⁶ CFU of *Listeria* intraperitoneally. To quantitate bacterial CFUs, spleens were harvested from infected mice and homogenized using FastPrep-24 5G (MP Biomedicals) in PBS containing 0.1% Triton X-100, followed by serial dilutions using PBS and plating onto BHI agar plates. Colonies were counted after 24 hours of growth at 37°C. The intracellular IFN-γ level in T cells was measured as described⁵⁰. Splenocytes were stimulated with 50 ng/ml phorbol 12-myristate 13-acetate and 1 μM ionomycin in the presence of 1 μg/mL brefeldin A for 4.5 hours, followed by staining with antibody against CD3. The cells were fixed with 2% paraformaldehyde, permeabilized with 0.1% saponin, and stained for IFN-γ, then IFN-γ levels were analyzed by flow cytometry in CD3⁺ cells. The mice were processed and data were collected in a manner blinded to sample identity.

Electrophysiology

Oln-mTomato⁺ cells were isolated by flow cytometry and cultured for 2 days in 6-well plates pre-coated with 100 ng/ml of fibronectin (Sigma), with DMEM-low glucose (Gibco) plus 20% fetal bovine serum (Sigma F2442), 10mM ROCK inhibitor (Y-27632, Selleck), and 1% penicillin/streptomycin (Invitrogen) at 37°C in a low oxygen environment (to promote cell survival) within gas-tight chambers (Billups-Rothenberg) flushed with 1% O₂ and 6% CO₂ (balance Nitrogen). After that, the cells were transferred to a regular 37°C incubator with 5% CO₂, cultured for 3 additional days, detached with TrypLE Express (Thermo Scientific) and replated on glass coverslides (Carolina Biological Supply) at 50–70% confluency for 16 hours before electrophysiological recordings. Single channel current recordings of endogenous Piezo1 were performed using an Axopatch 200B amplifier and

Digidata 1550B digitizer (Molecular Devices). Currents were acquired with pClamp 10.7 software at a sampling frequency of 10 kHz. Recording patch pipettes of borosilicate glass were pulled and fire-polished to a tip resistance of 4–6 M Ω . The external bath solution contained 140 mM KCl, 10 mM HEPES, 1 mM MgCl₂, 10 mM glucose, pH 7.3 (pH adjusted with KOH). The pipette solution contained: 130 mM NaCl, 5 mM KCl, 10 mM HEPES, 10mM tetraethylammonium chloride (TEA-Cl), 1m M CaCl₂, 1 mM MgCl₂, pH 7.3 (pH adjusted with NaOH). The bath electrode was grounded, while the pipette electrode was active, such that at positive applied potential, cations moved from pipette to bath, and vice versa. Mechanical stimulation was applied via recording pipette using a high-speed pressure clamp system (ALA Scientific Instruments). Single channel events are shown as upward deflections at +60 mV representing inward currents. The single channel data was analyzed using Clampfit 10.7. All point current histograms (ranging from 5–10 seconds recorded stretch) were constructed in Clampfit. The single channel current values were extracted after fitting the Gaussian function to the data. Data are presented as Mean \pm S.D. Each data point is at least an average of 5 to 10 individual recordings. Open probability was calculated exclusively from the records, where at least 10 seconds of data were recorded both before and after pressure application.

Statistical methods

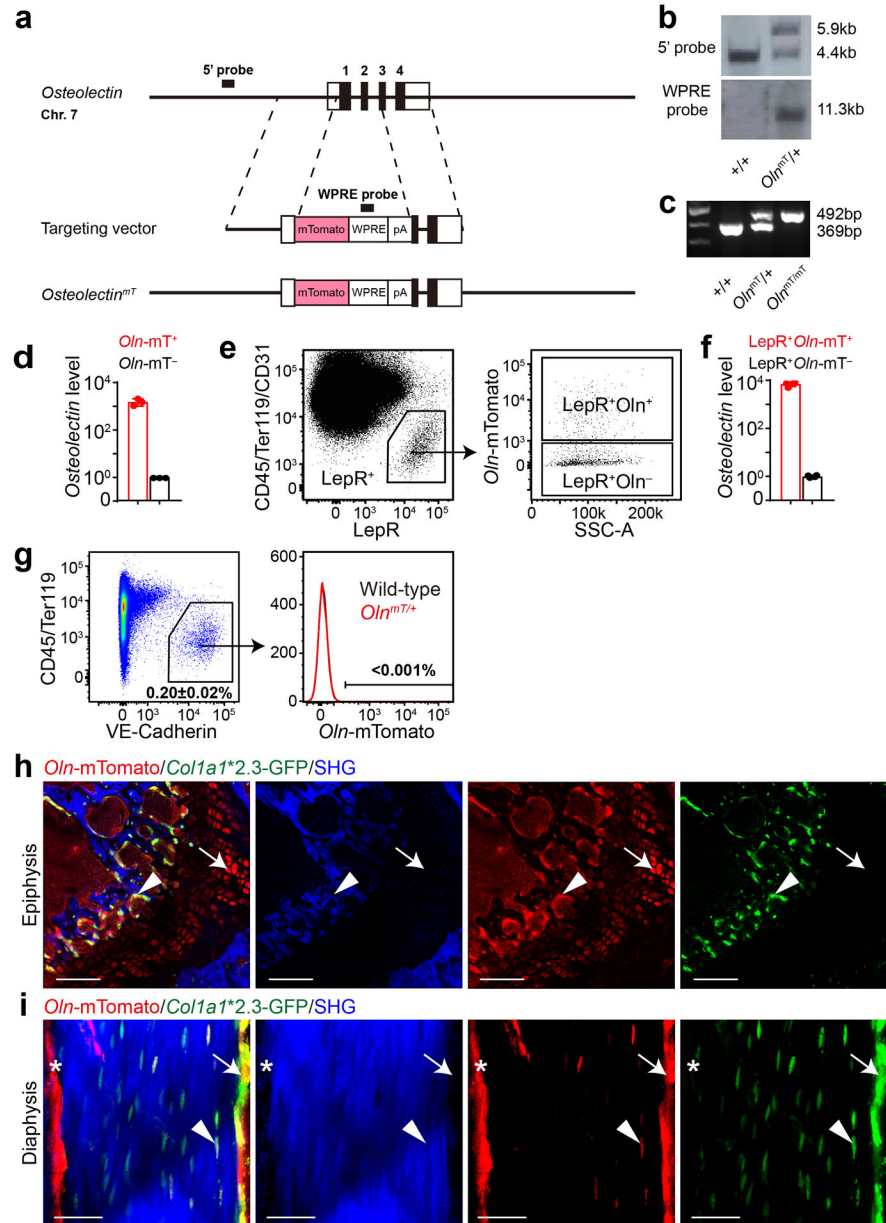
In each type of experiment, multiple independent experiments were performed using different mice on different days. Mice were allocated to experiments randomly and samples were processed in an arbitrary order, but formal randomization techniques were not used. Prior to analyzing the statistical significance of differences among treatments, we tested whether the data were normally distributed and whether variance was similar among treatments. To test for normal distribution, we performed the Shapiro–Wilk test when $3 < n < 20$ or the D’Agostino Omnibus test when $n \geq 20$. To test if variability significantly differed among treatments, we performed *F*-tests (for experiments with two treatments) or Levene’s median tests (for more than two treatments). When the data significantly deviated from normality or variability significantly differed among treatments, we log₂-transformed the data and tested again for normality and variability. If the transformed data no longer significantly deviated from normality and equal variability, we performed parametric tests on the transformed data. If transformed data still significantly deviated from normality or equal variability, we performed non-parametric tests on the non-transformed data.

All the statistical tests we used were two-sided, where applicable. To assess the statistical significance of a difference between two treatments, we used paired t-tests (when mice were littermates and a parametric test was appropriate), Wilcoxon signed rank tests (when mice were littermates and a non-parametric test was appropriate), t-tests (when mice were not littermates and a parametric test was appropriate), or Mann-Whitney tests (when mice were not littermates and a non-parametric test was appropriate). Multiple t-tests (parametric or non-parametric) were followed by Holm-Sidak’s multiple comparisons adjustment. To assess the statistical significance of differences between more than two treatments, we used repeated measures one-way or two-way ANOVAs (when mice were littermates and/or cells were from same mice, and a parametric test was appropriate) followed by Tukey’s, Dunnet’s, or Sidak’s multiple comparisons adjustment. To assess the significance of

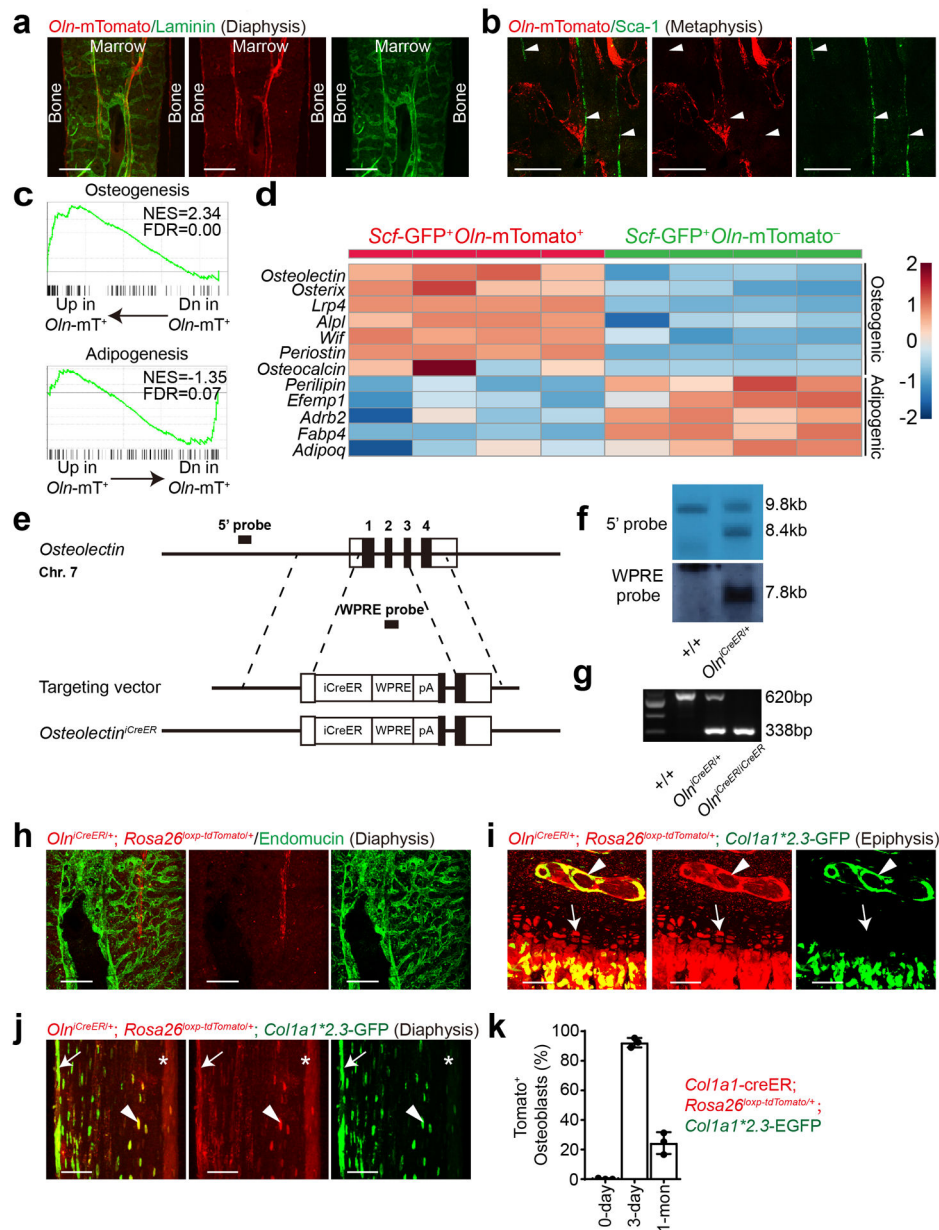
frequency differences within contingency tables that involved multiple experiments we used Cochran–Mantel–Haenszel tests. To assess the significance of survival differences we used the Mantel-Cox log-rank test.

All statistical analyses were performed with Graphpad Prism 8.3 or R 3.5.1 with the fBasics package. All data represent mean \pm standard deviation. Samples sizes were not pre-determined based on statistical power calculations but were based on our experience with these assays.

Extended Data



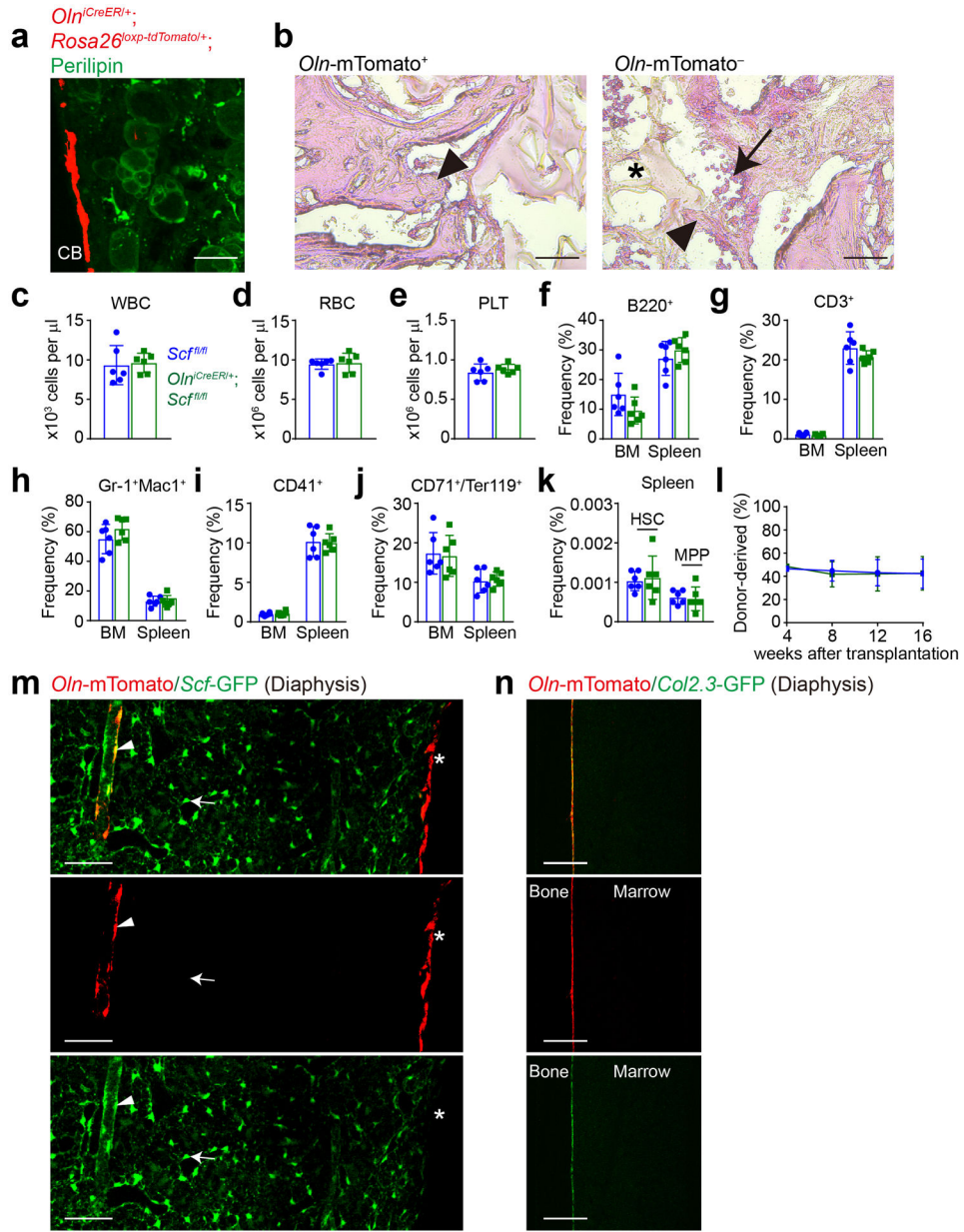
Extended Data Figure 1. *Oln^{mT}* reporter mice showed that Ostelectin is expressed by osteoblasts, osteocytes, and chondrocytes in addition to peri-arteriolar LepR⁺ stromal cells. (a-c) The mouse *Ostelectin* gene was modified to insert an mTomato-WPRE-pA cassette between the 5' untranslated region and exon 3 to generate the targeting vector. These sites were selected to avoid disrupting conserved intronic sequences. Open boxes indicate untranslated regions and black boxes indicate translated regions of *Ostelectin*. The targeted founder mouse (F0) was identified by southern blotting (b) using 5' and WPRE probes (black bars). (c) PCR genotyping of genomic DNA confirmed germline transmission of the *Oln^{mT}* allele. Mice were backcrossed at least three times onto a C57BL/Ka background before analysis. (d) *Ostelectin* transcript levels by qRT-PCR in *Oln*-Tomato⁺ and *Oln*-Tomato⁻ bone marrow cells (3 mice analyzed in 3 independent experiments). (e) Flow cytometry gates to distinguish *Oln*-mTomato⁺LepR⁺ from *Oln*-mTomato⁻LepR⁺ stromal cells in enzymatically dissociated bone marrow. (f) *Ostelectin* transcript levels by qRT-PCR in *Oln*-Tomato⁺LepR⁺ and *Oln*-Tomato⁻LepR⁺ bone marrow cells (4 mice analyzed in 4 independent experiments). (g) We did not detect *Oln*-Tomato in VE-cadherin-expressing bone marrow endothelial cells (4 mice per genotype analyzed in 4 independent experiments). (h and i) Femur epiphysis (h) and diaphysis (i) from *Oln^{mT}*⁺; *Colla1*2.3*-EGFP mice (images are representative of 3 independent experiments from 8–10-week-old mice). In panel h, the arrowhead points to *Oln*-Tomato⁺*Colla1*2.3*-EGFP⁺ osteoblasts in trabecular bone and the arrow points to *Oln*-Tomato⁺*Colla1*2.3*-EGFP⁻ hypertrophic chondrocytes in the growth plate (scale bar = 100μm). Panel i shows *Oln*-Tomato⁺*Colla1*2.3*-EGFP⁺ osteoblasts at the endosteum (arrow), *Oln*-Tomato⁺ osteocytes (arrowhead), and *Oln*-Tomato⁺ periosteal cells (asterisk) (scale bars = 40μm). All data represent mean ± SD.



Extended Data Figure 2. Bone marrow *Oln-mTomato*⁺ cells localized mainly around arterioles in the diaphysis.

(a) A low magnification view of the femur diaphysis showed *Oln-mTomato*⁺ stromal cells associated with arterioles enriched in the center of the marrow. In this image, arteriolar and sinusoidal blood vessels were distinguished based on size, morphology, and continuity of the basal lamina, visualized using anti-laminin antibody staining as previously described²¹ (images are representative of 3 independent experiments; scale bar = 200 μ m). (b) *Oln^{mT+}* femur bone marrow showing that, in contrast to the diaphysis (Fig. 1h), most Sca-1⁺ arterioles were not surrounded by *Oln-mTomato*⁺ stromal cells in the metaphysis. The *Oln-mTomato*⁺ cells in this panel were osteoblasts and osteocytes associated with trabecular bone (scale bar = 500 μ m). (c, d) Gene set enrichment analysis showing significant enrichment of genes associated with osteogenesis in CD45⁻Ter119⁻CD31⁻*Scf-GFP*⁺*Oln-mTomato*⁺

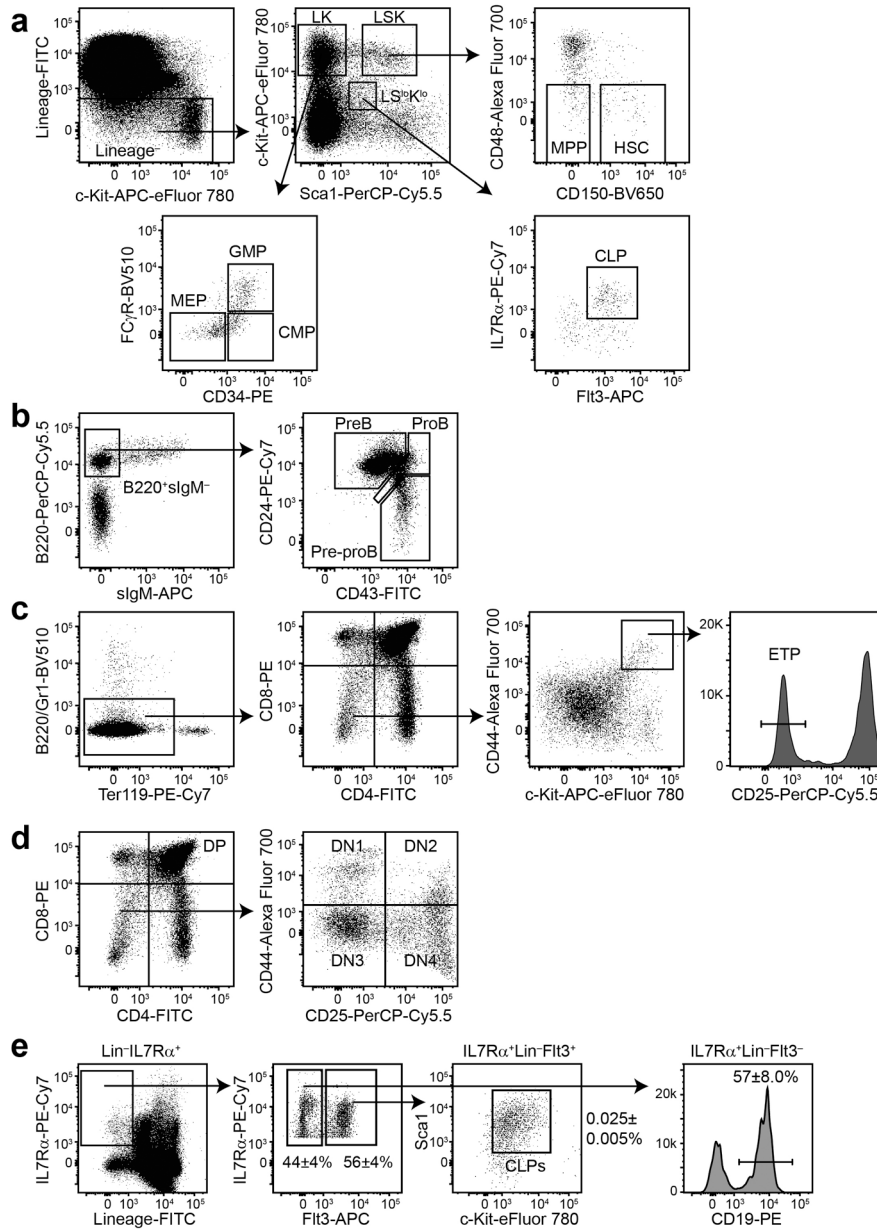
stromal cells and adipogenesis in CD45⁻Ter119⁻CD31⁻Scf-GFP⁺Oln-mTomato⁻ stromal cells (FDR, false discovery rate; NES, normalized enrichment score; 4 mice analyzed in 4 independent experiments). **(e-f)** The mouse *Ostelectin* gene was modified by inserting an iCreER-WPRE-pA cassette between the 5' untranslated region and exon 3 to generate the targeting vector. These sites were selected to avoid disrupting conserved intronic sequences. Open boxes indicate untranslated regions and black boxes indicate translated regions of *Ostelectin*. The targeted founder mouse (F0) was identified by Southern blotting **(f)** using 5' and WPRE probes (black bars). **(g)** PCR genotyping of genomic DNA confirmed germline transmission of the *Oln^{iCreER}* allele. Mice were backcrossed at least three times onto a C57BL/Ka background before analysis. **(h)** Deep imaging of *Oln^{iCreER}*; *Rosa26^{loxP-tdTomato}*^{+/+} femur bone marrow 3 days after tamoxifen administration at 2 months of age, showing that *Oln*-Tomato⁺ cells were exclusively peri-arteriolar in the diaphysis (images are representative of 3 independent experiments; scale bar = 200µm). **(i and j)** Deep imaging of the femur epiphysis **(i)** and diaphysis **(j)** one month after tamoxifen administration at 2 months of age (images are representative of 3 independent experiments). Panel **i** shows *Oln*-Tomato⁺ hypertrophic chondrocytes in the growth plate (arrow) and *Oln*-Tomato⁺*Col1a1**2.3-EGFP⁺ osteoblasts in trabecular bone (arrowhead; scale bar = 60µm). Panel **j** shows *Oln*-Tomato⁺*Col1a1**2.3-EGFP⁺ osteoblasts at the endosteum (arrow), an *Oln*-Tomato⁺ osteocyte (arrowhead), and *Oln*-Tomato⁺ periosteal cells (asterisk; scale bars = 30µm). **(k)** *Col1a1*-CreER; *Rosa26^{loxP-tdTomato}*^{+/+}; *Col1a1**2.3-EGFP mice were treated with tamoxifen at 2 months of age and the percentage of *Col1a1**2.3-EGFP⁺ osteoblasts that were Tomato⁺ was assessed 3 days to 1 month later (3 mice per time point analyzed in 3 independent experiments). All data represent mean ± SD.



Extended Data Figure 3. Ostelectin⁺ cells create a niche for CLPs but not other hematopoietic stem/progenitor cells.

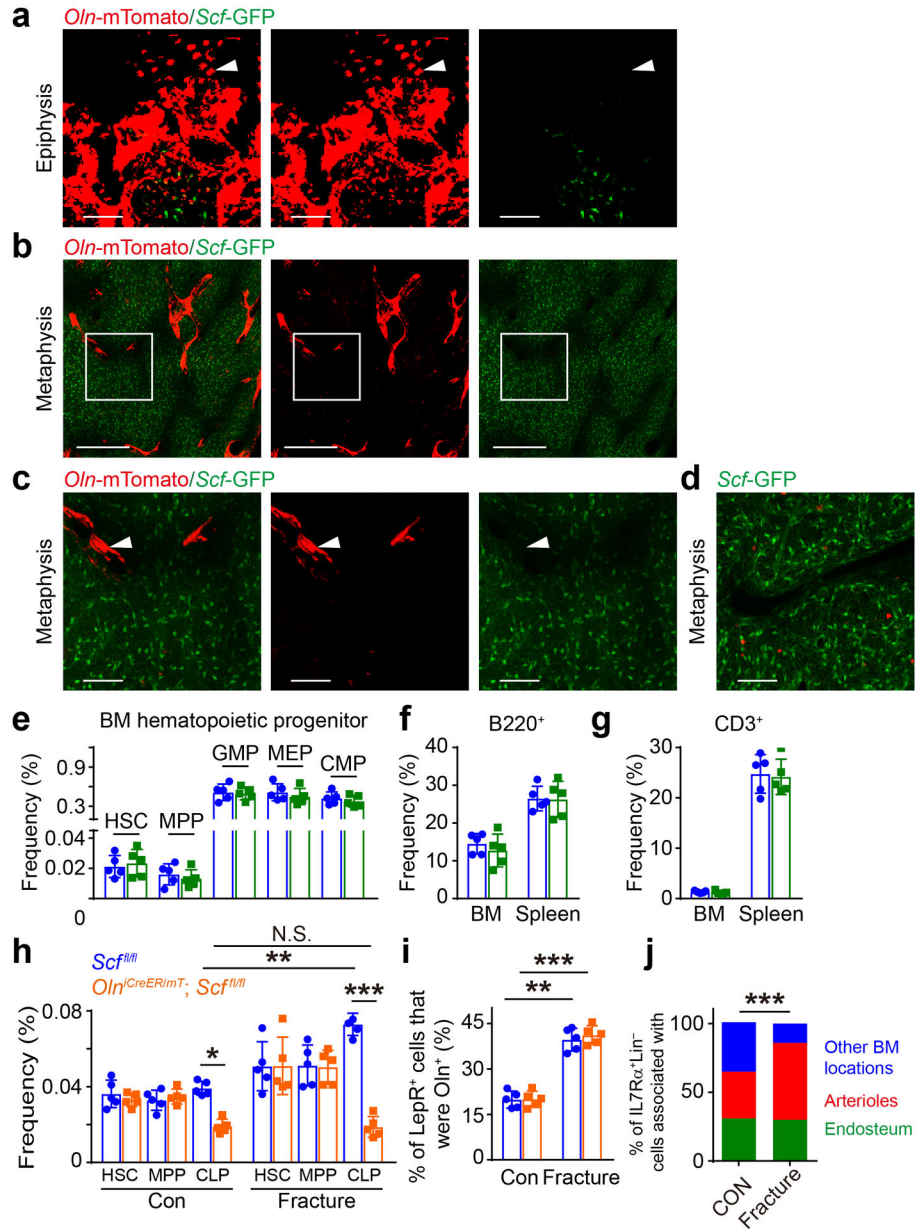
(a) 2-month-old *Oln^{iCreER/+}; Rosa26^{loxP-tdTomato/+}* mice were sublethally irradiated 3 days after tamoxifen administration. Two weeks later, none of the adipocytes in the bone marrow were Tomato⁺ (image representative of 3 independent experiments; scale bar = 60μm). (b) Representative H&E stained sections from ossicles formed by *Oln-Tomato⁺* (left) or *Oln-Tomato⁻* (right) stromal cells sorted from *Oln^{mT/+}* mice showing bone (arrowheads), hematopoietic cells (arrow), and adipocytes (asterisk; images are representative of 5 independent experiments; scale bar = 100μm). (c-e) *Oln^{iCreER/+}; Scf^{fl/fl}* and *Scf^{fl/fl}* littermate controls were treated with tamoxifen at 2-months of age. One month later, blood from *Oln^{iCreER/+}; Scf^{fl/fl}* mice showed normal white blood cell (c), red blood cell (d) and platelet (e) counts (6 mice per genotype analyzed in 3 independent experiments). (f-k) *Oln^{iCreER/+}*;

Scf^{fl/fl} mice and littermate controls exhibited no significant differences in the frequencies of B220⁺ B cells (**f**), CD3⁺ T cells (**g**), Gr-1⁺Mac-1⁺ myeloid cells (**h**), CD41⁺ megakaryocyte lineage cells (**i**), CD71⁺/Ter119⁺ erythroid lineage cells (**j**), HSCs or MPPs in the spleen (**k**; 6 mice per genotype analyzed in 3 independent experiments). (**l**) Bone marrow cells from *Oln^{iCreER/+}*; *Scf^{fl/fl}* mice and littermate controls gave similar levels of donor cell reconstitution upon competitive transplantation into irradiated mice (5 donor mice per genotype analyzed in 3 independent experiments). The differences between *Oln^{iCreER/+}*; *Scf^{fl/fl}* and *Scf^{fl/fl}* mice were not statistically significant in **c-l**. (**m**) *Oln^{mT/+}*; *Scf^{GFP/+}* femur bone marrow showing *Oln*-Tomato⁺ osteoblasts at the endosteum were negative for *Scf*-GFP, while peri-arteriolar *Oln*-Tomato⁺ stromal cells were positive for *Scf*-GFP (representative of 3 independent experiments; scale bar = 80μm). (**n**) *Oln^{mT/+}*; *Col1a1*2.3*-EGFP femur bone marrow showing *Col1a1*2.3*-EGFP⁺ osteoblasts at the endosteum were *Oln*-Tomato⁺ (representative of 3 independent experiments; scale bar = 100μm). All data represent mean ± SD. Statistical significance was assessed using matched samples two-way ANOVAs followed by Sidak's (**c-e**, and **k-l**) or Tukey's (**f-j**) multiple comparisons tests.



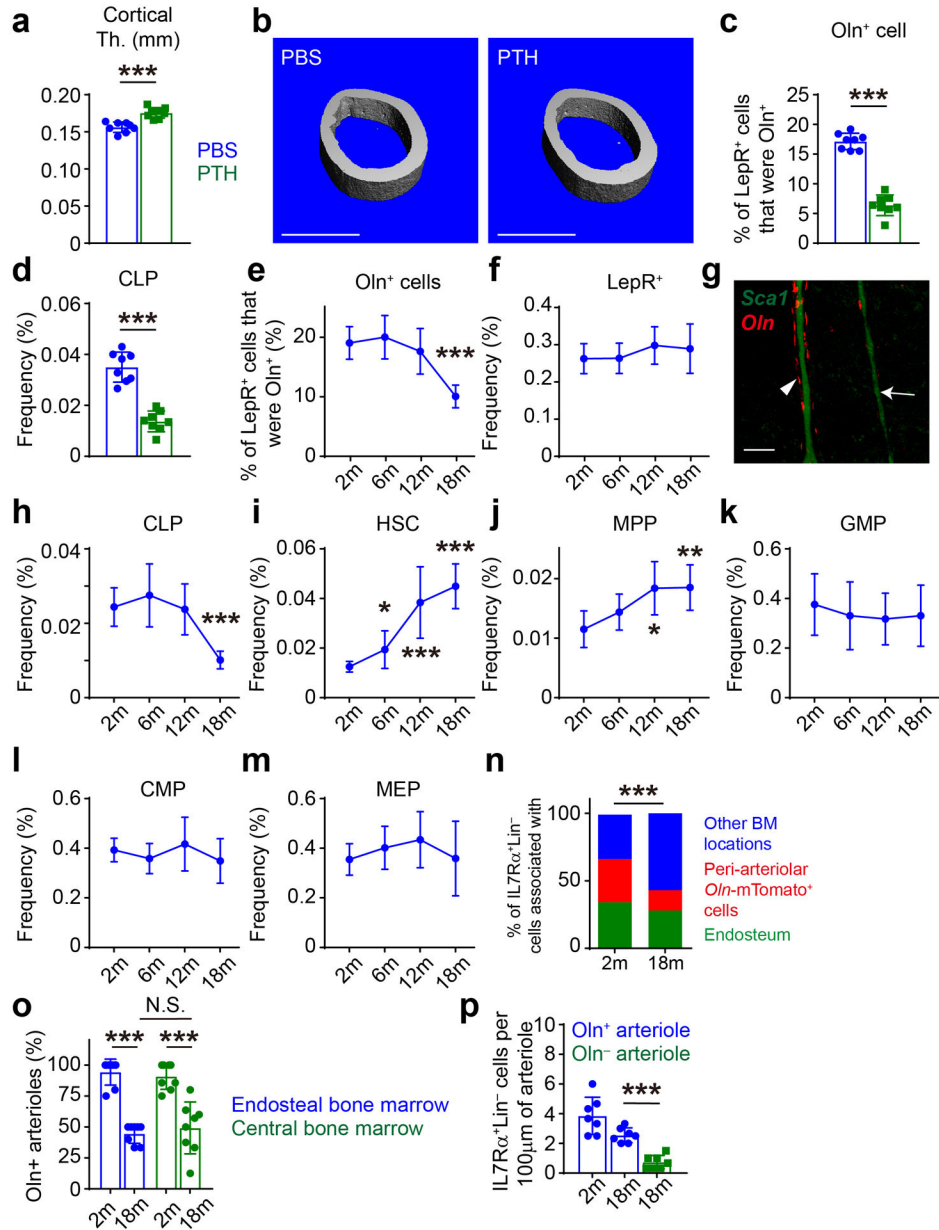
Extended Data Figure 4. Flow cytometry gating strategy for the isolation of hematopoietic stem and progenitor cell populations.

(a-d) Representative flow cytometry gates used to identify the hematopoietic stem and progenitor cell populations in the bone marrow (a, b), and T lineage progenitors in the thymus (c, d). The markers used to identify each of the cell populations characterized in this study are listed in Supplementary Table 1. (e) Representative flow cytometry gates showing that more than 50% of IL7Rα⁺Lineage⁻ cells were Lin⁻Sca1^{low}c-kit^{low}IL7Rα⁺Fit3⁺ CLPs and most of the non-CLP IL7Rα⁺Lineage⁻ (Fit3⁻) cells were CD19⁺, likely to be other early B lineage progenitors (4 mice analyzed in 3 independent experiments). All data represent mean ± SD.



Extended Data Figure 5. *Oln-mTomato*⁺ osteoblasts and osteocytes in the metaphysis do not express *Scf-GFP* and *Oln-mTomato*⁺ cells in the diaphysis expand during fracture healing. The differences among treatments in cell frequencies were also evident in absolute numbers. (a-c) Epiphysis (a) and metaphysis (b, c) of *Oln^{mT/+}; Scf^{GFP/+}* femur bone marrow showing that hypertrophic chondrocytes (arrowhead in a; scale bars = 30 μ m) as well as osteoblasts and osteocytes associated with trabecular bone (arrowhead in c) were negative for *Scf-GFP* (images are representative of 3 independent experiments; scale bars = 400 μ m (b) and 100 μ m (c)). Most of the *Oln-Tomato* staining in the metaphysis reflects *Col1a1^{*2.3-GFP}* osteoblasts and osteocytes associated with trabecular bone, as shown in Fig. 1d and Extended Data Fig. 2b. The boxed area in panel b is magnified in panel c. (d) Image of the metaphysis of *Scf^{GFP/+}* femur bone marrow showing limited non-specific staining by anti-

tdTomato antibody (scale bar = 100mm). **(e-g)** *Oln^{iCreER/+}*; *Scf^{fl/fl}* and *Scf^{fl/fl}* littermate control mice were fed tamoxifen chow from 2–4 months of age. They exhibited no significant differences in the frequencies of HSCs, MPPs, GMPs, MEPs, or CMPs in the bone marrow **(e)**, or B220⁺ B cells **(f)**, or CD3⁺ T cells **(g)** in the bone marrow or spleen. The differences between *Oln^{iCreER/+}*; *Scf^{fl/fl}* and *Scf^{fl/fl}* mice were not statistically significant in **e-g** (5 mice per genotype analyzed in 3 independent experiments). **(h, i)** Three days after tamoxifen, femurs were fractured in 2-month-old *Oln^{mT/iCreER}*; *Scf^{fl/fl}* mice and *Oln^{mT/+}*; *Scf^{fl/fl}* littermate controls then the bone marrow was analyzed two weeks later. HSC and MPP frequencies did not significantly change during fracture healing. In contrast, CLP frequencies significantly increased in *Oln^{mT/+}*; *Scf^{fl/fl}* control but not in *Oln^{mT/iCreER}*; *Scf^{fl/fl}* mice **(h)**. The frequency of Ostelectin⁺ cells significantly increased in both *Oln^{mT/iCreER}*; *Scf^{fl/fl}* mice and *Oln^{mT/+}*; *Scf^{fl/fl}* controls **(I)**; 5 mice per genotype analyzed in 3 independent experiments). **(j)** Localization of IL7R α ⁺Lineage⁻ lymphoid progenitors in the marrow of the fractured as compared to control (CON) femur (4 mice per treatment analyzed in 4 independent experiments). All data represent mean \pm SD. Statistical significance was assessed using matched samples two-way ANOVAs followed by Sidak's **(e-i)** or Tukey's multiple comparisons tests **(h)**, or Cochran-Mantel-Haenszel test **(j)**.

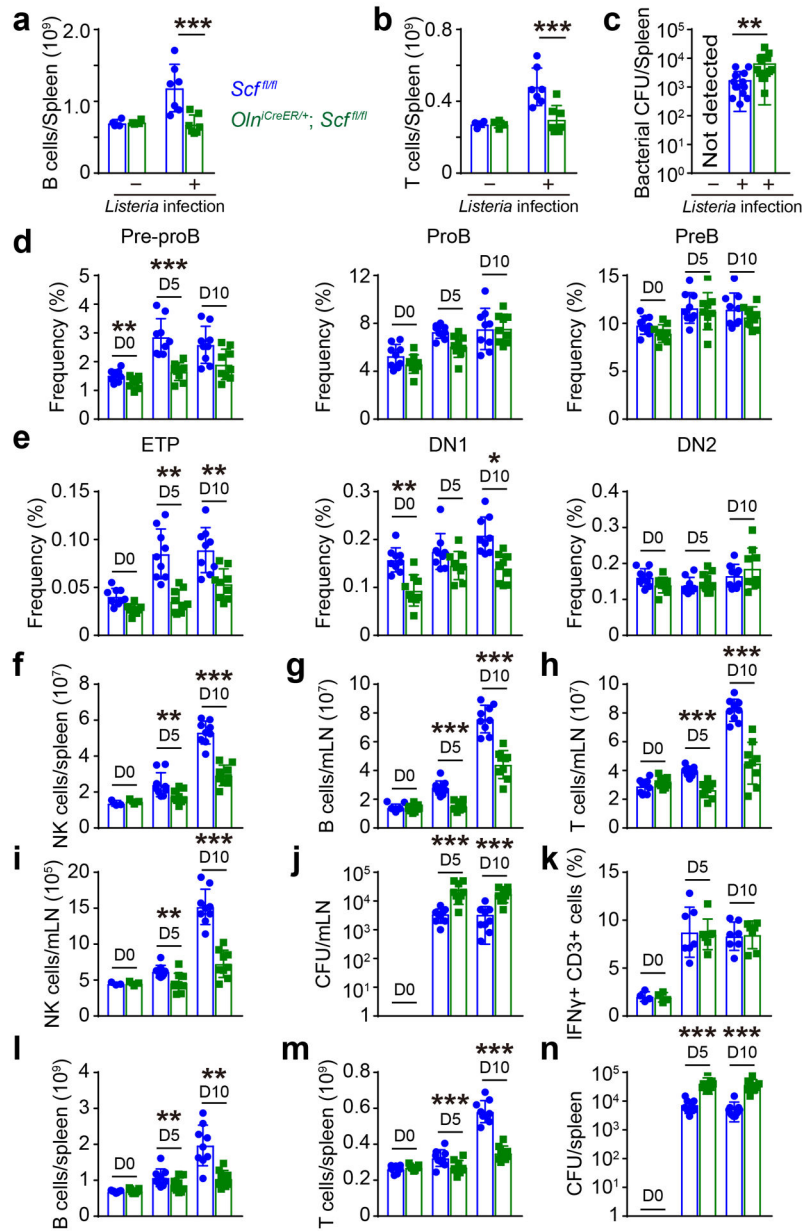


Extended Data Figure 6. CLPs and peri-arteriolar Osteoclast⁺ cells are depleted during aging but most other hematopoietic stem and progenitor cell populations are not.

The differences among treatments in cell frequencies were also evident in absolute numbers.

(a-d) *Oln^{mT/+}* mice received daily subcutaneous injections with PBS or 40 μg/kg human PTH for 28 days. PTH treated mice exhibited significantly thicker cortical bone (a, b) and significant reductions in the frequencies of Osteoclast⁺ cells (c) and CLPs (d; 8 mice per treatment analyzed in 4 independent experiments). Micro CT images (b, scale bar = 800μm) of cortical bone are representative of 8 independent experiments. (e, f) The frequency of LepR⁺ cells (e) and the percentage of LepR⁺ cells that were *Oln*-mTomato⁺ (f) in *Oln^{mT/+}* bone marrow at 2 to 18 months of age (8 mice per time point analyzed in 4 independent experiments). (g) Femur bone marrow from an 18-month-old *Oln^{mT/+}* mouse showing an arteriole surrounded by *Oln*-mTomato⁺ cells (arrowhead) and an arteriole lacking *Oln*-

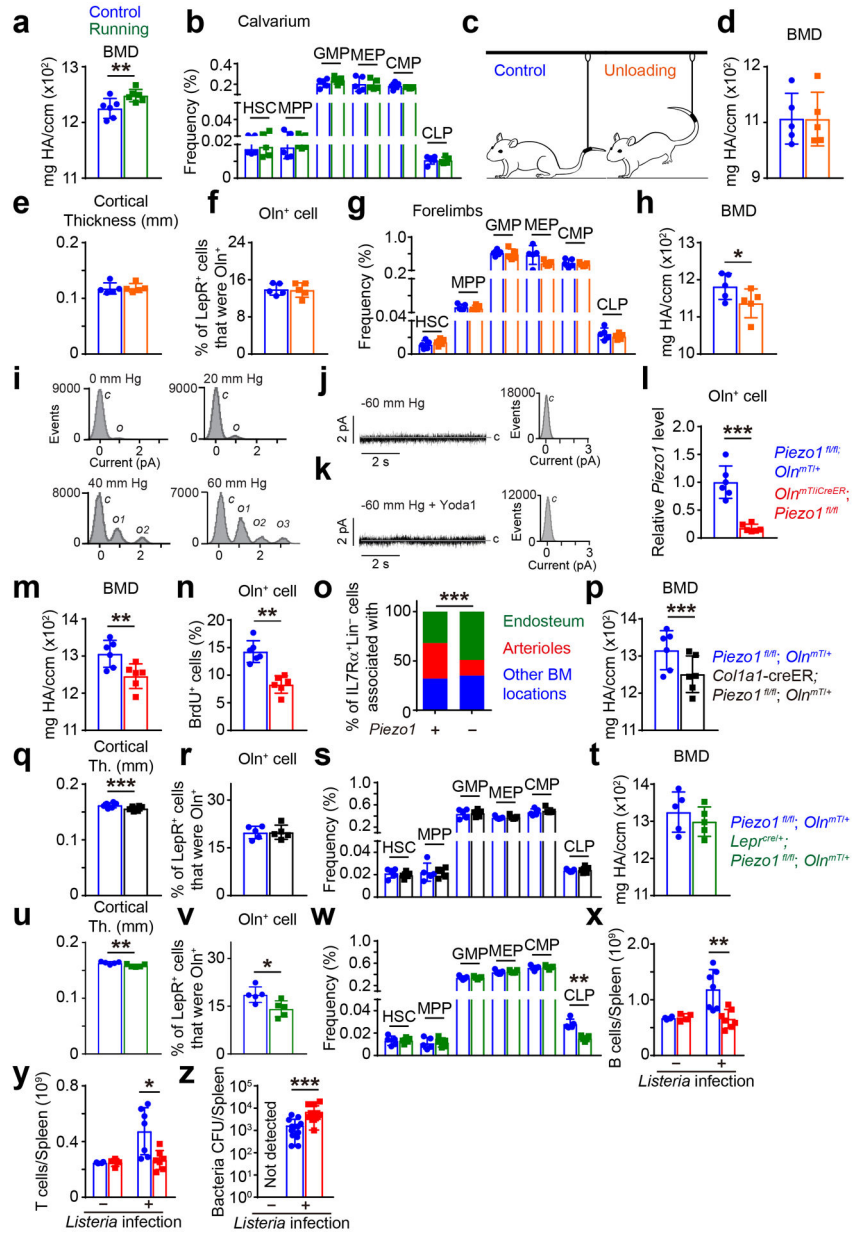
mTomato⁺ cells (arrow) in the diaphysis (image is representative of 4 independent experiments; scale bar = 100μm). **(h)** The frequency of CLPs in *Oln^{mT/+}* mice at 2 to 18 months of age. **(i-m)** During aging, the frequencies of HSCs **(i)** and MPPs **(j)** in the bone marrow increased while the frequencies of GMPs **(k)**, CMPs **(l)**, and MEPs **(m)** did not significantly change (8 mice per time point analyzed in 4 independent experiments). **(n)** Localization of IL7Rα⁺Lineage⁻ cells in the bone marrow of 2- and 18-month old mice (7 mice per time point analyzed in 3 independent experiments). **(o)** Aging significantly depleted Ostelectin⁺ cells associated with arterioles in both endosteal and non-endosteal regions of diaphysis bone marrow (8 mice per time point analyzed in 4 independent experiments). **(p)** Number of IL7Rα⁺Lineage⁻ cells per 100 μm of Ostelectin⁺ or Ostelectin⁻ arteriole at 2 and 18 months of age (7 mice per time point analyzed in 3 independent experiments). All data represent mean ± SD. Statistical significance was assessed using paired *t*-tests **(a, c, d, o, p)**, one-way ANOVA followed by Dunnett's multiple comparisons test **(e)**, matched samples two-way ANOVAs followed by Dunnett's multiple comparisons tests **(f, h-m)**, Cochran-Mantel-Haenszel test **(n)**, or Mann-Whitney tests followed by Holm-Sidak's multiple comparisons adjustments **(o)**.



Extended Data Figure 7. *Oln^{iCreER/+}; Scf^{fl/fl}* mice exhibited reduced lymphopoiesis and impaired bacterial clearance after *Listeria* infection.

The same differences that were evident among treatments in the frequencies of cell populations were also evident in absolute numbers. (a-c) *Oln^{iCreER/+}; Scf^{fl/fl}* mice and littermate controls were treated with tamoxifen at 2 months of age and then 3 days later were administered *Listeria* orally. Relative to *Scf^{fl/fl}* littermate controls, *Oln^{iCreER/+}; Scf^{fl/fl}* mice had decreased B (a) and T (b) cell counts in the spleen 5 days after *Listeria* infection and increased bacterial CFUs in the spleen 10 days after infection (c; 11–16 mice per genotype analyzed in 3 independent experiments). (d-k) *Oln^{iCreER/+}; Scf^{fl/fl}* and *Scf^{fl/fl}* littermate controls were fed tamoxifen from 2 to 4-months of age then 3 days later were administered *Listeria* intraperitoneally. Relative to *Scf^{fl/fl}* littermate controls, *Oln^{iCreER/+}; Scf^{fl/fl}* mice exhibited reduced frequencies of Pre-proB cells, but not ProB or PreB cells, in the bone

marrow (**d**) as well as ETPs and DN1 cells in the thymus (**e**) at 5 and/or 10 days after infection. *Oln^{iCreER/+}; Scf^{fl/fl}* mice also exhibited reduced numbers of NK cells in the spleen (**f**) as well as B cells (**g**), T cells (**h**), and NK cells (**i**) in mesenteric lymph nodes (mLN) at 5 and 10 days after infection. (**j**) *Oln^{iCreER/+}; Scf^{fl/fl}* mice exhibited increased bacterial CFUs in mLN at 5 and 10 days after infection. (**k**) The percentage of CD3⁺ T cells that were IFN- γ ⁺ did not significantly differ between the spleens of *Oln^{iCreER/+}; Scf^{fl/fl}* mice and littermate controls (18–27 mice per genotype analyzed in 3 independent experiments). (**l-n**) Compared to *Scf^{fl/fl}* controls, *Oln^{iCreER/+}; Scf^{fl/fl}* mice had decreased spleen B (**l**) and T (**m**) cell counts, and increased spleen bacterial CFUs (**n**) at 5 and 10 days after infection with *Listeria* (21–27 mice per genotype analyzed in 3 independent experiments). All data represent mean \pm SD. Statistical significance was assessed using matched samples two-way ANOVAs followed by Sidak's multiple comparisons tests (**a**, **b**, **d-n**) or Wilcoxon matched-pairs test (**c**).



Extended Data Figure 8. Mechanical stimulation is required for the maintenance of peri-arteriolar, but not peri-sinusoidal, niches for lymphoid progenitors in the bone marrow.

(a) The effect of voluntary running for 4 weeks on femoral cortical bone mineral density (6 mice per treatment analyzed in 3 independent experiments). (b) Voluntary running for 4 weeks did not significantly affect the frequencies of HSCs, MPPs, GMPs, MEPs, CMPs, or CLPs in calvarium bone marrow (5 mice per treatment analyzed in 3 independent experiments). (c-h) Hindlimb unloading (c) for 2 weeks did not significantly affect forelimb cortical bone mineral density (d), cortical thickness (e), the percentage of LepR⁺ cells that were *Oln*-mTomato⁺ (f), or the frequencies of HSCs, MPPs, GMPs, MEPs, CMPs, or CLPs in humerus bone marrow (g). (h) Hindlimb unloading for 2 weeks did significantly reduce hindlimb (femur) cortical bone mineral density (5 mice per treatment analyzed in 3

independent experiments). **(i)** All point current amplitude histograms of the electrical recordings in Fig. 4h. The single channel conductance was 15 ± 1 pS from the Gaussian fits to the amplitude histograms. The y-axis shows the number of events. **(j, k)** Single channel current recordings and corresponding all point current histograms of *Piezo1* deficient *Oln*^{mTomato} cells isolated from *Oln*^{mT*i*CreER}; *Piezo1*^{fl/fl} mice. The data were collected at -60 mm Hg applied pressure and at the holding potential of +60 mV, without **(j)** or with **(k)** 40 μ M Yoda1 in the pipette. **(l)** *Piezo1* transcript levels by qRT-PCR in *Oln*-Tomato⁺ cells from *Oln*^{mT*i*CreER}; *Piezo1*^{fl/fl} and *Oln*^{mT/+}; *Piezo1*^{fl/fl} control mice (6 mice per genotype analyzed in 3 independent experiments). **(m and n)** The effect of *Piezo1* deletion in Ostelectin⁺ cells on femoral cortical bone mineral density **(m)** and the percentage of Ostelectin⁺ cells that incorporated a 48 hour pulse of BrdU **(n)**; 6 mice per genotype analyzed in 3 independent experiments). **(o)** Location of IL7R α ⁺Lineage⁻ cells in the bone marrow of *Oln*^{mT*i*CreER}; *Piezo1*^{fl/fl} and *Oln*^{mT/+}; *Piezo1*^{fl/fl} control mice (6 mice per genotype analyzed in 3 independent experiments). **(p-s)** We treated *Colla1*-creER; *Piezo1*^{fl/fl}; *Oln*^{mT/+} mice and littermate controls with tamoxifen at 2 months of age and analyzed them 1 month later. *Piezo1* deletion in osteoblasts significantly reduced femur bone mineral density **(p)** and cortical thickness **(q)** but not the frequencies of Ostelectin⁺ cells **(r)** or HSCs, MPPs, GMPs, MEPs, or CLPs in the bone marrow **(s)**; 5–6 mice per genotype analyzed in 3 independent experiments). **(t-w)** We analyzed the femurs of *Lep^rcre/+*; *Piezo1*^{fl/fl}; *Oln*^{mT/+} mice and littermate controls at 4 months of age and found that *Piezo1* deletion in LepR⁺ cells did not significantly reduce bone mineral density **(t)** but did reduce cortical thickness **(u)**. *Piezo1* deletion in LepR⁺ cells also significantly reduced the frequencies of Ostelectin⁺ cells **(v)** and CLPs **(w)** without affecting the frequencies of HSCs, MPPs, GMPs, MEPs, or CMPs **(w)** in the bone marrow (5 mice per genotype analyzed in 3 independent experiments). **(x-z)** Compared to *Scf*^{fl/fl} littermate controls, *Oln*^{iCreER/+}; *Piezo1*^{fl/fl} mice had decreased B **(x)** and T **(y)** cell counts in the spleen 5 days after oral *Listeria* infection and increased bacterial CFUs in the spleen 10 days after infection **(z)**; 11–16 mice per genotype analyzed in 3 independent experiments). All data represent mean \pm SD. Statistical significance was assessed using paired t-tests **(a, l, m, n, p-r, t-v, z)**, matched samples two-way ANOVAs followed by Sidak's **(b, d-f, h, s, w-y)** or Holm-Sidak's multiple comparisons adjustment **(g)**, or Cochran-Mantel-Haenszel test **(o)**.

Supplementary Material

Refer to Web version on PubMed Central for supplementary material.

ACKNOWLEDGEMENTS

S.J.M. is a Howard Hughes Medical Institute (HHMI) Investigator, the Mary McDermott Cook Chair in Pediatric Genetics, the Kathryn and Gene Bishop Distinguished Chair in Pediatric Research, the director of the Hamon Laboratory for Stem Cells and Cancer, and a Cancer Prevention and Research Institute of Texas Scholar. This work was supported partly by the National Institutes of Health (DK11875 to S.J.M.). B.S. was supported by a Ruth L. Kirschstein National Research Service Award Postdoctoral Fellowship from the National Heart, Lung, and Blood Institute (F32 HL139016-01). A.T. was supported by the Leopoldina Fellowship Program (LPDS 2016-16) of the German National Academy of Sciences and the Fritz Thyssen Foundation. L.A.J. was supported by ARC Discovery grants (DP200101970, DE190100609). R.S. was supported by the UT Southwestern Medical Center Endowed Scholar Program, Welch Foundation Award (I-1965-20180324), and an American Heart Association scientist development grant (17SDG33410184). We thank H. Zeng (Allen Institute) and H. Taniguchi (Max Planck Florida Institute) for providing the *Ai47* mice. We thank N. Loof, T. Shih, and the Moody Foundation Flow Cytometry

Facility. We thank the BioHPC high performance computing cloud at UT Southwestern Medical Center for providing computational resources.

REFERENCES

1. Ding L, Saunders TL, Enikolopov G & Morrison SJ Endothelial and perivascular cells maintain haematopoietic stem cells. *Nature* 481, 457–462, (2012). [PubMed: 22281595]
2. Ding L & Morrison SJ Haematopoietic stem cells and early lymphoid progenitors occupy distinct bone marrow niches. *Nature* 495, 231–235, (2013). [PubMed: 23434755]
3. Oguro H, Ding L & Morrison SJ SLAM family markers resolve functionally distinct subpopulations of hematopoietic stem cells and multipotent progenitors. *Cell Stem Cell* 13, 102–116, (2013). [PubMed: 23827712]
4. Cordeiro Gomes A et al. Hematopoietic Stem Cell Niches Produce Lineage-Instructive Signals to Control Multipotent Progenitor Differentiation. *Immunity* 45, 1219–1231, (2016). [PubMed: 27913094]
5. Himburg HA et al. Distinct Bone Marrow Sources of Pleiotrophin Control Hematopoietic Stem Cell Maintenance and Regeneration. *Cell Stem Cell* 23, 370–381 e375, (2018). [PubMed: 30100167]
6. Comazetto S et al. Restricted Hematopoietic Progenitors and Erythropoiesis Require SCF from Leptin Receptor+ Niche Cells in the Bone Marrow. *Cell Stem Cell* 24, 477–486 e476, (2019). [PubMed: 30661958]
7. Zhou BO, Yue R, Murphy MM, Peyer JG & Morrison SJ Leptin-receptor-expressing mesenchymal stromal cells represent the main source of bone formed by adult bone marrow. *Cell Stem Cell* 15, 154–168, (2014). [PubMed: 24953181]
8. Zhou BO et al. Bone marrow adipocytes promote the regeneration of stem cells and haematopoiesis by secreting SCF. *Nat Cell Biol* 19, 891–903, (2017). [PubMed: 28714970]
9. Tikhonova AN et al. The bone marrow microenvironment at single-cell resolution. *Nature* 569, 222–228, (2019). [PubMed: 30971824]
10. Baryawno N et al. A Cellular Taxonomy of the Bone Marrow Stroma in Homeostasis and Leukemia. *Cell* 177, 1915–1932 e1916, (2019). [PubMed: 31130381]
11. Baccin C et al. Combined single-cell and spatial transcriptomics reveal the molecular, cellular and spatial bone marrow niche organization. *Nat Cell Biol*, (2019).
12. Matsushita Y et al. A Wnt-mediated transformation of the bone marrow stromal cell identity orchestrates skeletal regeneration. *Nat Commun* 11, 332, (2020). [PubMed: 31949165]
13. Yue R, Shen B & Morrison SJ Clec11a/osteolectin is an osteogenic growth factor that promotes the maintenance of the adult skeleton. *Elife* 5, e18782, (2016). [PubMed: 27976999]
14. Shen B et al. Integrin alpha11 is an Osteolectin receptor and is required for the maintenance of adult skeletal bone mass. *Elife* 8, e42274, (2019). [PubMed: 30632962]
15. Crane GM, Jeffery E & Morrison SJ Adult haematopoietic stem cell niches. *Nat Rev Immunol* 17, 573–590, (2017). [PubMed: 28604734]
16. Greenbaum A et al. CXCL12 in early mesenchymal progenitors is required for haematopoietic stem-cell maintenance. *Nature* 495, 227–230, (2013). [PubMed: 23434756]
17. Sacma M et al. Haematopoietic stem cells in perisinusoidal niches are protected from ageing. *Nat Cell Biol* 21, 1309–1320, (2019). [PubMed: 31685996]
18. Young K et al. Progressive alterations in multipotent hematopoietic progenitors underlie lymphoid cell loss in aging. *J Exp Med* 213, 2259–2267, (2016). [PubMed: 27811054]
19. Kusumbe AP et al. Age-dependent modulation of vascular niches for haematopoietic stem cells. *Nature* 532, 380–384, (2016). [PubMed: 27074508]
20. Kiel MJ et al. SLAM family receptors distinguish hematopoietic stem and progenitor cells and reveal endothelial niches for stem cells. *Cell* 121, 1109–1121, (2005). [PubMed: 15989959]
21. Acar M et al. Deep imaging of bone marrow shows non-dividing stem cells are mainly perisinusoidal. *Nature* 526, 126–130, (2015). [PubMed: 26416744]
22. Christodoulou C et al. Live-animal imaging of native haematopoietic stem and progenitor cells. *Nature* 578, 278–283, (2020). [PubMed: 32025033]

23. Visnjic D et al. Hematopoiesis is severely altered in mice with an induced osteoblast deficiency. *Blood* 103, 3258–3264, (2004). [PubMed: 14726388]
24. Zhu J et al. Osteoblasts support B-lymphocyte commitment and differentiation from hematopoietic stem cells. *Blood* 109, 3706–3712, (2007). [PubMed: 17227831]
25. Kusumbe AP, Ramasamy SK & Adams RH Coupling of angiogenesis and osteogenesis by a specific vessel subtype in bone. *Nature* 507, 323–328, (2014). [PubMed: 24646994]
26. Kalajzic Z et al. Directing the expression of a green fluorescent protein transgene in differentiated osteoblasts: comparison between rat type I collagen and rat osteocalcin promoters. *Bone* 31, 654–660, (2002). [PubMed: 12531558]
27. Dobnig H & Turner RT Evidence that intermittent treatment with parathyroid hormone increases bone formation in adult rats by activation of bone lining cells. *Endocrinology* 136, 3632–3638, (1995). [PubMed: 7628403]
28. Park D et al. Endogenous bone marrow MSCs are dynamic, fate-restricted participants in bone maintenance and regeneration. *Cell Stem Cell* 10, 259–272, (2012). [PubMed: 22385654]
29. Bianco P, Kuznetsov SA, Riminucci M & Gehron Robey P Postnatal skeletal stem cells. *Methods Enzymol* 419, 117–148, (2006). [PubMed: 17141054]
30. Morrison SJ, Wandycz AM, Akashi K, Globerson A & Weissman IL The aging of hematopoietic stem cells. *Nat Med* 2, 1011–1016, (1996). [PubMed: 8782459]
31. Ladel CH, Flesch IE, Arnoldi J & Kaufmann SH Studies with MHC-deficient knock-out mice reveal impact of both MHC I- and MHC II-dependent T cell responses on *Listeria monocytogenes* infection. *J Immunol* 153, 3116–3122, (1994). [PubMed: 7726898]
32. Kayraklioglu N, Horuluoglu B, Elango M & Klinman DM Critical Role of B Cells in Toll-Like Receptor 7-Mediated Protection against *Listeria monocytogenes* Infection. *Infect Immun* 87, (2019).
33. Robling AG et al. Mechanical stimulation of bone in vivo reduces osteocyte expression of Sost/sclerostin. *J Biol Chem* 283, 5866–5875, (2008). [PubMed: 18089564]
34. Li X et al. Stimulation of Piezo1 by mechanical signals promotes bone anabolism. *Elife* 8, e49631, (2019). [PubMed: 31588901]
35. Sun W et al. The mechanosensitive Piezo1 channel is required for bone formation. *Elife* 8, e47454, (2019). [PubMed: 31290742]
36. Iwaniec UT & Turner RT Influence of body weight on bone mass, architecture and turnover. *J Endocrinol* 230, R115–130, (2016). [PubMed: 27352896]
37. Coste B et al. Piezo1 and Piezo2 are essential components of distinct mechanically activated cation channels. *Science* 330, 55–60, (2010). [PubMed: 20813920]
38. Wang L et al. Mechanical sensing protein PIEZO1 regulates bone homeostasis via osteoblast-osteoclast crosstalk. *Nat Commun* 11, 282, (2020). [PubMed: 31941964]
39. Coste B et al. Piezo proteins are pore-forming subunits of mechanically activated channels. *Nature* 483, 176–181, (2012). [PubMed: 22343900]
40. Syeda R et al. Chemical activation of the mechanotransduction channel Piezo1. *Elife* 4, (2015).
41. Boron WF & Boulpaep EL *Medical Physiology*. Chapter 19; Page 473 (2009).
42. Gruneboom A et al. A network of trans-cortical capillaries as mainstay for blood circulation in long bones. *Nat Metab* 1, 236–250, (2019). [PubMed: 31620676]
43. Sivaraj KK & Adams RH Blood vessel formation and function in bone. *Development* 143, 2706–2715, (2016). [PubMed: 27486231]
44. DeFalco J et al. Virus-assisted mapping of neural inputs to a feeding center in the hypothalamus. *Science* 291, 2608–2613, (2001). [PubMed: 11283374]
45. Madisen L et al. A robust and high-throughput Cre reporting and characterization system for the whole mouse brain. *Nat Neurosci* 13, 133–140, (2010). [PubMed: 20023653]
46. Daigle TL et al. A Suite of Transgenic Driver and Reporter Mouse Lines with Enhanced Brain-Cell-Type Targeting and Functionality. *Cell* 174, 465–480 e422, (2018). [PubMed: 30007418]
47. Cahalan SM et al. Piezo1 links mechanical forces to red blood cell volume. *Elife* 4, e07370, (2015).

48. Muzumdar MD, Tasic B, Miyamichi K, Li L & Luo L A global double-fluorescent Cre reporter mouse. *Genesis* 45, 593–605, (2007). [PubMed: 17868096]
49. Morrison SJ et al. Culture in reduced levels of oxygen promotes clonogenic sympathoadrenal differentiation by isolated neural crest stem cells. *J Neurosci* 20, 7370–7376, (2000). [PubMed: 11007895]
50. Gao D et al. Activation of cyclic GMP-AMP synthase by self-DNA causes autoimmune diseases. *Proc Natl Acad Sci U S A* 112, E5699–5705, (2015). [PubMed: 26371324]

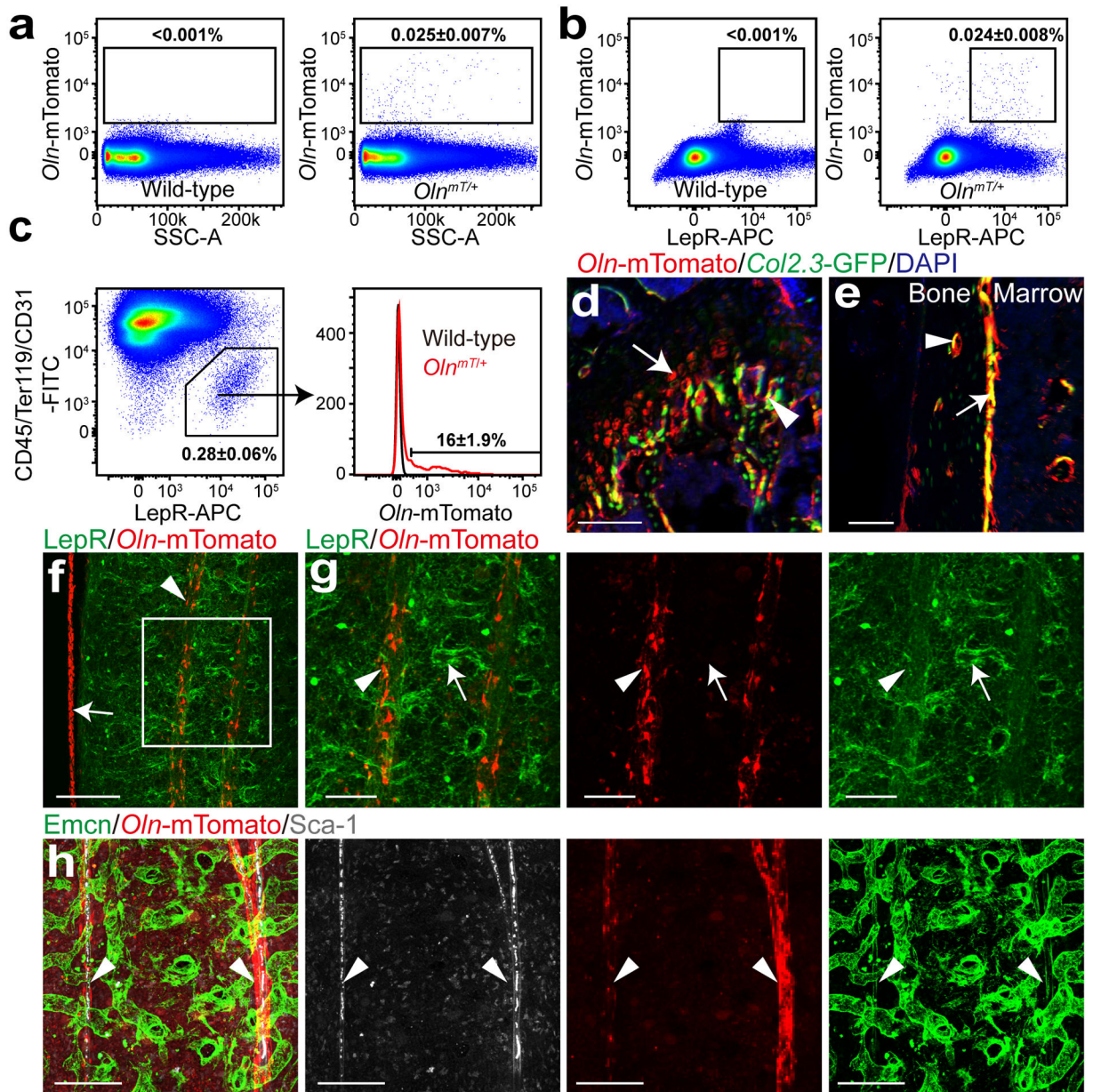


Figure 1. Ostelectin is expressed by peri-arteriolar LepR⁺ cells.

Images are representative of 3–5 experiments with 8–10-week-old mice. (a–c) Flow cytometric analysis of enzymatically dissociated bone marrow from *Oln^{mT/+}* mice (4 mice per genotype in 4 independent experiments). (b) Most *Oln-Tomato*⁺ cells were LepR⁺. (c) Only a small minority of LepR⁺ cells were *Oln-Tomato*⁺. (d and e) Representative femur sections showing the epiphysis (d) and diaphysis (e) from 2–4-month-old *Oln^{mT/+}; Colla1*2.3-EGFP* mice. Panel d shows *Oln-Tomato*⁺ hypertrophic chondrocytes (arrow) and *Oln-Tomato*⁺ *Colla1*2.3-EGFP*⁺ osteoblasts in trabecular bone (arrowhead; scale bar = 30μm). Panel e shows *Oln-Tomato*⁺ *Colla1*2.3-EGFP*⁺ osteoblasts in the endosteum (arrow) and *Oln-Tomato*⁺ osteocytes (arrowhead; scale bars = 25μm). (f and g) Deep imaging of *Oln^{mT/+}* femur bone marrow. The boxed area in panel f is magnified in panel g. Panel f

shows peri-arteriolar *Oln*-Tomato⁺ cells (arrowhead) as well as *Oln*-Tomato⁺ cells on the endosteal surface (arrow; scale bar = 100μm). Panel **g** shows *Oln*-Tomato⁺LepR⁺ peri-arteriolar stromal cells (arrowhead) and *Oln*-Tomato⁻LepR⁺ peri-sinusoidal stromal cells (arrow; scale bar = 40μm). (**h**) *Oln*-Tomato⁺ cells around Sca-1⁺ arterioles (arrow) but not Endomucin^{high} sinusoids (scale bar = 200μm). All data represent mean ± SD.

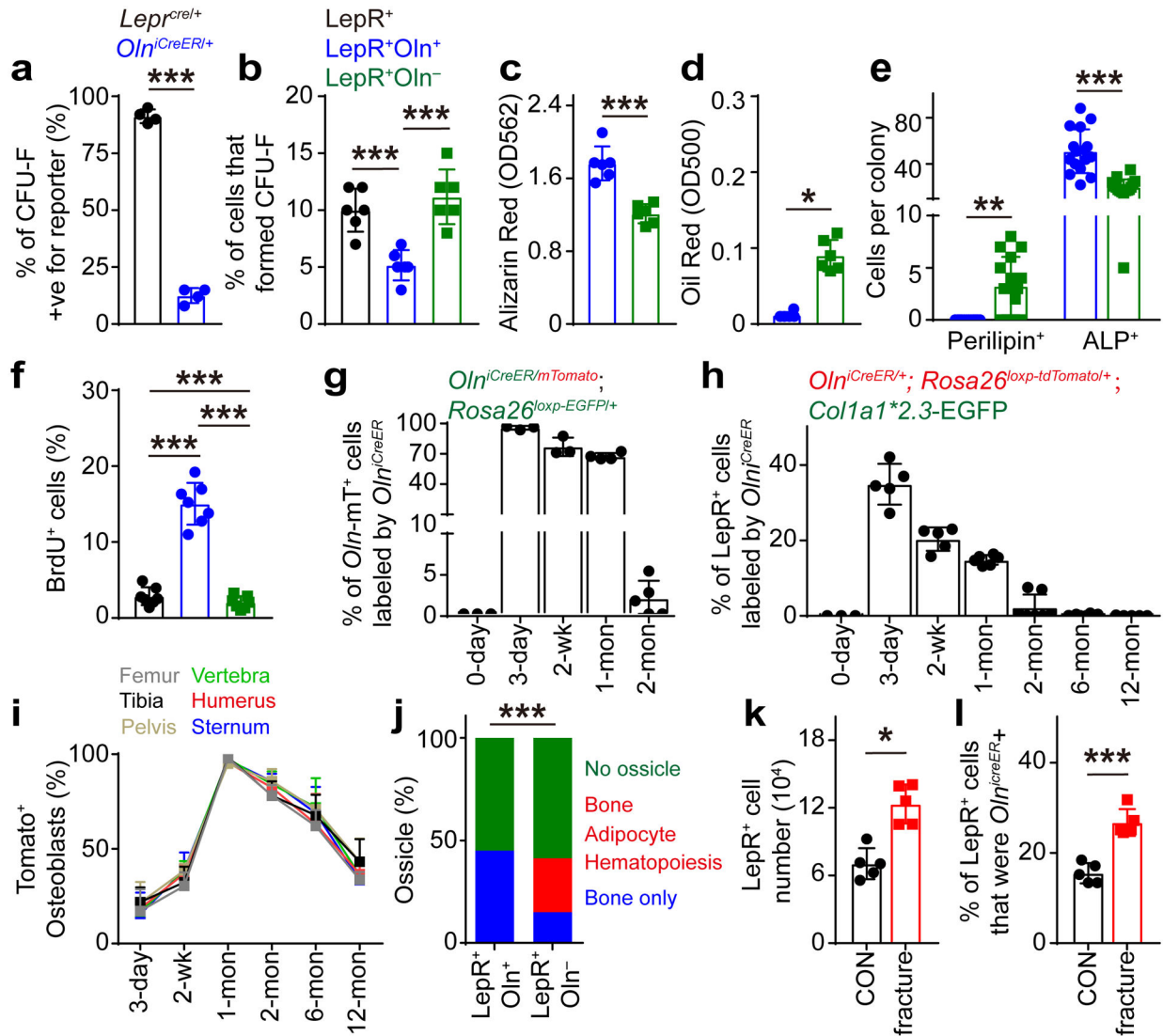


Figure 2. Ostelectin⁺ cells are short-lived osteogenic progenitors.

(a) Percentage of CFU-F colonies that were Tomato⁺ when formed by bone marrow cells from 2 month-old *LepR^{cre/+}; Rosa26^{loxp-tdTomato/+}* or *Oln^{iCreER/+}; Rosa26^{loxp-tdTomato/+}* mice, 3 days after tamoxifen administration (4 independent experiments). (b) Percentage of LepR⁺, LepR⁺*Oln-mTomato*⁺, and LepR⁺*Oln-mTomato*⁻ bone marrow stromal cells that formed CFU-F colonies. (c and d) Osteogenic (c) and adipogenic (d) differentiation of adherent cells cultured from LepR⁺*Oln-mTomato*⁺ or LepR⁺*Oln-mTomato*⁻ stromal cells (6 independent experiments in b-d). (e) The average numbers of perilipin⁺ adipocytes or alkaline phosphatase⁺ (ALP⁺) osteogenic cells that spontaneously differentiated per CFU-F colony after 1 week of culture (4 independent experiments). (f) Percentage of LepR⁺, LepR⁺*Oln-mTomato*⁺ and LepR⁺*Oln-mTomato*⁻ bone marrow stromal cells that incorporated a 24-hour pulse of BrdU in vivo (4 independent experiments). (g) *Oln^{iCreER/mT}; Rosa26^{loxp-EGFP/+}* mice were treated with tamoxifen at 2 months of age and the percentage of *Oln-mTomato*⁺ cells that were EGFP⁺ was assessed (3 independent experiments). (h and i) *Oln^{iCreER/+}; Rosa26^{loxp-tdTomato/+}; Col1a1*2.3-EGFP* mice were treated with tamoxifen at 2

months of age and the percentages of LepR⁺ stromal cells (**h**) and *Col1a1**2.3-EGFP⁺ osteoblasts (**i**) that were Tomato⁺ was assessed (5 independent experiments). (**j**) Bone, adipocytes, and hematopoiesis in ossicles formed by CFU-F cultured from LepR⁺*Oln*-mTomato⁺ or LepR⁺*Oln*-mTomato⁻ stromal cells (80 ossicles per cell population derived from 20 mice in 5 independent experiments). (**k-l**) Femurs were fractured 3 days after tamoxifen administration to *Oln*^{CreER}+/+, *Rosa26*^{loxP-tdTomato}+/+, *Col1a1**2.3-EGFP mice. Two weeks later the number of LepR⁺ cells per femur (**k**) and the percentage of LepR⁺ cells that were Tomato⁺ (**l**) were assessed (5 independent experiments). All data represent mean ± SD. Statistical significance was assessed using an unpaired *t*-test (**a**), paired *t*-tests (**c, k, l**), matched samples one-way ANOVAs followed by Tukey's multiple comparisons tests (**b, f**), Wilcoxon test (**d**), Wilcoxon test followed by Holm-Sidak's multiple comparisons adjustment (**e**), or Cochran-Mantel-Haenszel test (**j**).

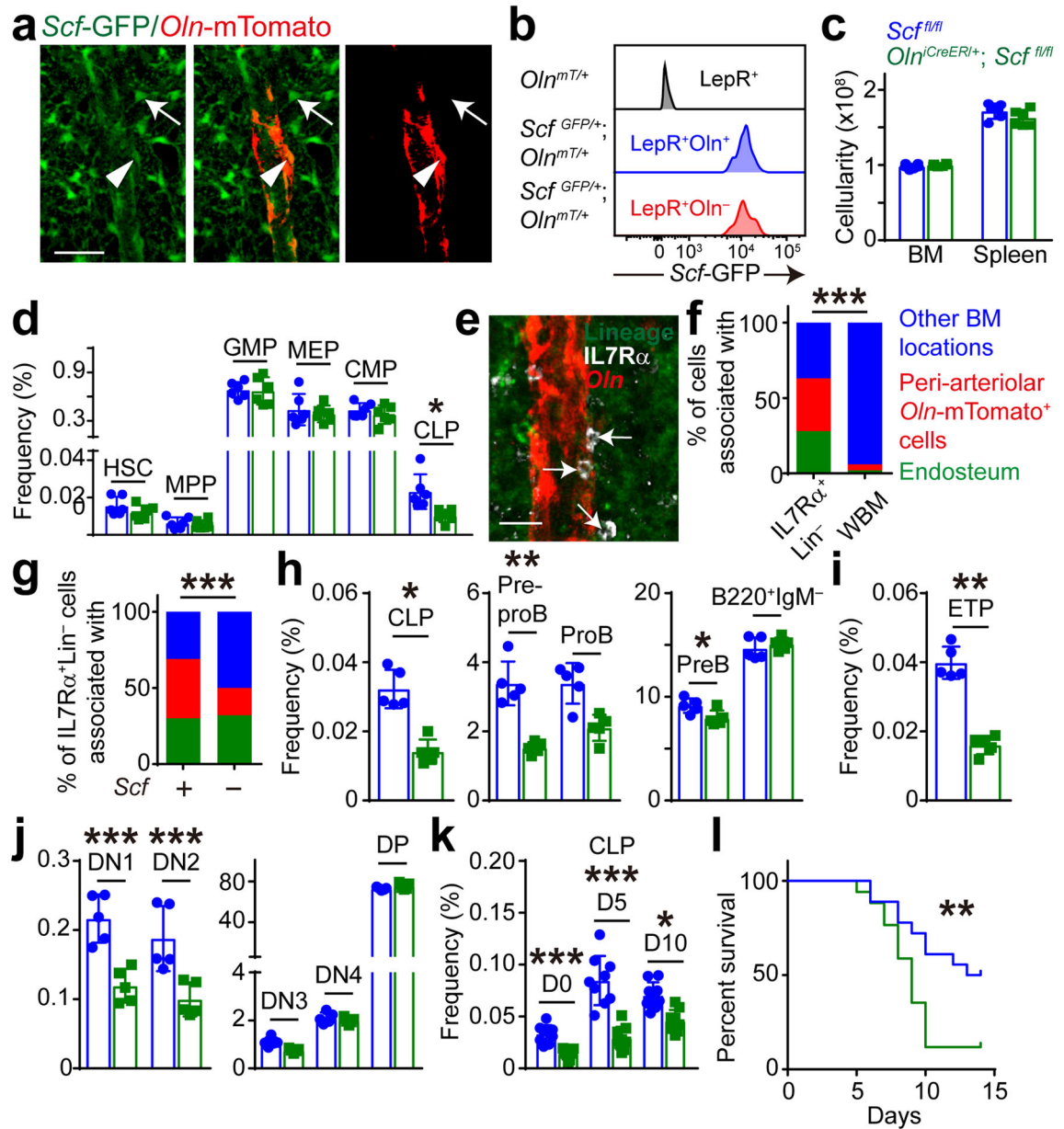


Figure 3. Osteoclastin⁺ peri-arteriolar stromal cells maintain early lymphoid progenitors by synthesizing SCF.

Images are representative of 3 independent experiments. The same differences that were evident among the frequencies of cell populations were also evident in absolute numbers. (a, b) In femur bone marrow from 2-month-old *Scf^{GFP/+}; Oln^{mT/+}* mice, *Scf*-GFP was expressed by both *Oln*-mTomato⁺ peri-arteriolar cells (arrowhead in a) and *Oln*-mTomato⁻ peri-sinusoidal cells (arrow in a; scale bar = 20µm). (c-d) *Oln^{iCreER/+}; Scf^{f1/f1}* and *Scf^{f1/f1}* littermate control mice were treated with tamoxifen at 2-months of age then bone marrow and spleen cellularity (c), and hematopoietic stem and progenitor cell frequencies in the bone marrow (d) were analyzed one month later (3 independent experiments). (e, f) Localization of IL7Rα⁺Lineage⁻ lymphoid progenitors (arrows) adjacent to peri-arteriolar

Ostelectin⁺ cells (scale bar = 15µm; 9 mice in 3 independent experiments). **(g)** Localization of IL7Rα⁺Lineage⁻ cells in the bone marrow of *Oln^{iCreER/+}; Scf^{fl/fl}* and *Scf^{fl/fl}* littermate control mice (6 mice per genotype in 3 independent experiments). **(h-j)** *Oln^{iCreER/+}; Scf^{fl/fl}* mice and littermate controls were fed tamoxifen from 2–4 months of age and the bone marrow **(h)** and thymus **(i, j)** were analyzed (3 independent experiments). **(k and l)** Compared to *Scf^{fl/fl}* controls, *Oln^{iCreER/+}; Scf^{fl/fl}* mice had decreased CLP frequency in the bone marrow **(k)** and worse survival **(l)** after *Listeria* infection (17–27 mice per genotype in 3 independent experiments). All data represent mean ± SD. Statistical significance was assessed using matched samples two-way ANOVAs followed by Sidak's multiple comparisons tests **(c, d, h-k)**, Cochran-Mantel-Haenszel tests **(f, g)**, or Mantel-Cox test **(l)**.

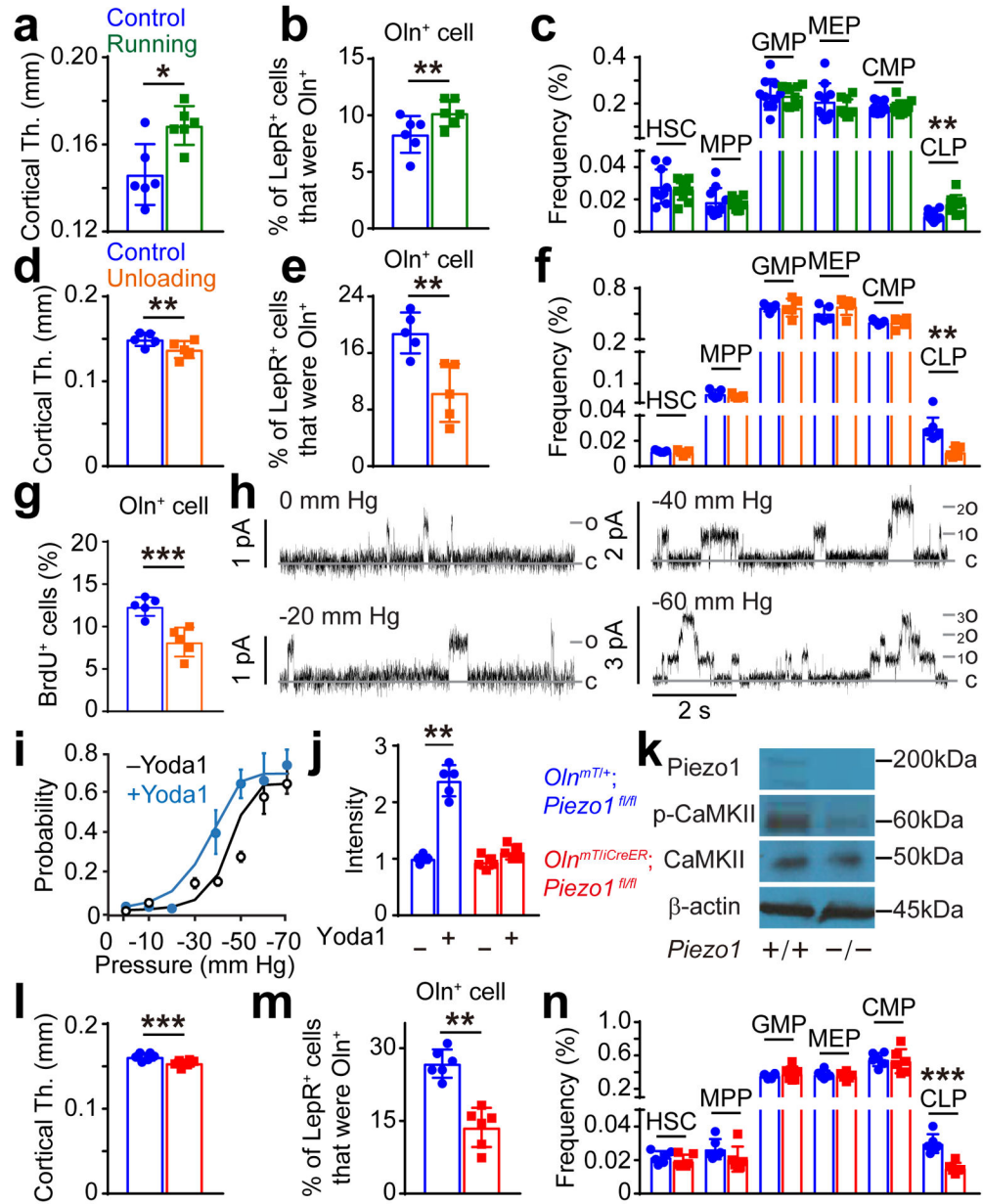


Figure 4. Mechanical stimulation is required for the maintenance of peri-arteriolar niches for lymphoid progenitors in the bone marrow.

The same differences that were evident among the frequencies of cell populations were also evident in absolute numbers. (a-c) The effect of voluntary running for 4 weeks on femoral cortical thickness (a), the percentage of LepR⁺ cells that were *Oln*-mTomato⁺ (b), and the frequencies of hematopoietic stem and progenitor cells in the bone marrow (c; 6–10 mice per treatment in 3–5 independent experiments). (d-g) The effect of hindlimb unloading for 2 weeks on femur cortical thickness (d), the percentage of LepR⁺ cells that were *Oln*-mTomato⁺ (e), the frequencies of stem and progenitors cells in the bone marrow (f), and the percentage of Osteoclast⁺ cells that incorporated a 48 hour pulse of BrdU (g; 5 mice per treatment in 3 independent experiments). (h) Single channel current recordings in *Oln*-

mTomato⁺ cells at the indicated applied pressures. O and C denote the open and closed states of the channels. **(i)** Normalized open probability–pressure relationship from *Oln*-mTomato⁺ cells recorded with (blue) or without (white) 40 μM Yoda1 in the patch pipette (6 mice in 6 independent experiments). **(j)** Yoda1 mediated Ca⁺⁺ response in *Oln*-mTomato⁺ cells isolated from *Oln*^{mT/iCreER}; *Piezo1*^{fl/fl} or *Oln*^{mT/+}; *Piezo1*^{fl/fl} littermate control mice (5 mice per genotype in 3 independent experiments). **(k)** Western blot of Ostelectin⁺ cells from *Oln*^{mT/iCreER}; *Piezo1*^{fl/fl} or *Oln*^{mT/+}; *Piezo1*^{fl/fl} mice (representative of three independent experiments). **(l-n)** The effect of *Piezo1* deletion in Ostelectin⁺ cells on cortical thickness **(l)**, the percentage of LepR⁺ cells that were *Oln*-mTomato⁺ **(m)**, and the frequencies of stem and progenitor cells in bone marrow **(n; 6 mice per genotype in 3 independent experiments)**. All data represent mean ± SD. Statistical significance was assessed using paired *t*-tests **(a, b, g, l, m)** and matched samples two-way ANOVAs followed by Sidak's **(c-e, j, n)** or Holm-Sidak's **(f)** multiple comparisons adjustments.